

1 **Tissue damage during acute *Trypanosoma cruzi* infection is**  
2 **associated with reduced reparative regulatory T cell response**  
3 **and can be attenuated by early interleukin-33 administration.**

4

5 **Short title: Reparative regulatory T cell response in *T. cruzi* infection.**

6

7 Santiago Boccardo<sup>1,2</sup>, Constanza Rodriguez<sup>1,2</sup>, Cintia L. Araujo Furlan<sup>1,2</sup>, Carolina P. Abrate<sup>1,2</sup>,

8 Laura Almada<sup>1,2</sup>, Camila M. S. Giménez<sup>1,2</sup>, Manuel A. Saldivia Concepción<sup>3</sup>, Peter Skewes-Cox<sup>3</sup>,

9 Srinivasa P. S. Rao<sup>3</sup>, Carolina L. Montes<sup>1,2</sup>, Adriana Gruppi<sup>1,2</sup>, Eva V. Acosta Rodríguez<sup>1,2#</sup>.

10

11 <sup>1</sup> Departamento de Bioquímica Clínica, Facultad de Ciencias Químicas, Universidad Nacional de  
12 Córdoba. Córdoba, Argentina.

13 <sup>2</sup> Centro de Investigaciones en Bioquímica Clínica e Inmunología, CONICET. Córdoba, Argentina.

14 <sup>3</sup> BioMedical Research, Novartis, Emeryville, California, United States.

15

16 # Corresponding author:

17 E-mail: [eva.acosta@unc.edu.ar](mailto:eva.acosta@unc.edu.ar) (EVAR)

## 18 ABSTRACT

19 Tissue-repair regulatory T cells (trTregs) constitute a specialized regulatory subset renowned for  
20 orchestrating tissue homeostasis and repair. While extensively investigated in sterile injury  
21 models, their role in infection-induced tissue damage and the regulation of protective  
22 antimicrobial immunity remains largely unexplored. This investigation examines trTregs  
23 dynamics during acute *Trypanosoma cruzi* infection, a unique scenario combining extensive  
24 tissue damage with robust antiparasitic CD8+ immunity. Contrary to conventional models of  
25 sterile injury, our findings reveal a pronounced reduction of trTregs in secondary lymphoid  
26 organs and tissues during acute *T. cruzi* infection. This unexpected decline correlates with  
27 systemic as well local tissue damage, as evidenced by histological alterations and  
28 downregulation of repair-associated genes in skeletal muscle. Remarkably, a parallel decrease  
29 in systemic levels of IL-33, a crucial factor for trTregs survival and expansion, was detected. We  
30 found that early treatment with systemic recombinant IL-33 during infection induces a notable  
31 surge in trTregs, accompanied by an expansion of type 2 innate lymphoid cells and parasite-  
32 specific CD8+ cells. This intervention results in a mitigated tissue damage profile and reduced  
33 parasite burden in infected mice. These findings shed light on trTregs biology during infection-  
34 induced injury and demonstrate the feasibility of enhancing a specialized Tregs response  
35 without impairing the magnitude of effector immune mechanisms, ultimately benefiting the  
36 host. Furthermore, this study settles groundwork of relevance for potential therapeutic  
37 strategies in Chagas' disease and other infections.

38

## 39 AUTHOR SUMMARY

40 Chagas' disease, caused by the protozoan *Trypanosoma cruzi*, induces severe organ damage  
41 caused by the interplay between the parasite and the immune response. In our investigation,

42 we delved into the role of tissue-repair regulatory T cells (trTregs) during the acute phase of *T.*  
43 *cruzi* infection in mice. Surprisingly, we observed a reduction in trTregs during the peak of tissue  
44 damage, contrary to their usual accumulation after injury in other contexts. This decline aligned  
45 with decreased levels of interleukin-33, a critical factor for trTregs survival. Administering  
46 interleukin-33 at early infection times not only boosted trTregs but also expanded other  
47 reparative and antiparasitic immune cells. Consequently, these treated mice exhibited reduced  
48 damage and lower parasite levels in tissues. Our findings offer insights into trTregs' behavior  
49 during infection-induced injury, suggesting a promising avenue for therapeutic interventions in  
50 Chagas' disease and related conditions. This study lays the groundwork for potential strategies  
51 that balance the immune response, supporting tissue repair without compromising the ability  
52 to control the infection, which could have broader implications for infectious diseases and tissue  
53 damage-related pathologies.

54

## 55 INTRODUCTION

56 Regulatory T cells (Tregs) are CD4+ T lymphocytes with immunoregulatory properties  
57 characterized by the expression of the transcription factor Forkhead box P3 (Foxp3) [1]. The  
58 immunomodulatory role of Tregs has been extensively described across diverse biological  
59 processes, encompassing tolerance maintenance, autoimmunity and allergy, as well as cancer,  
60 infectious and immunometabolic diseases [2]. This wide spectrum of activities underscores the  
61 adaptability of Tregs in regulating various effector responses, including Th1, Th2, and Th17  
62 immunity. This phenomenon, recognized as Tregs specialization, enables them to tailor their  
63 regulatory capacity to distinct scenarios and the specific immune profiles requiring modulation  
64 [3].

65 Recently, it has been identified a separate subset of Tregs that goes beyond their classic  
66 suppressive function to specialize in maintaining tissue homeostasis and promoting repair

67 following damage [4]. These cells, referred to as tissue repair Tregs (trTregs), were initially  
68 believed to be confined to non-immune tissues, but have subsequently been found in lymphoid  
69 organs as well [5]. Tissue repair Tregs exhibit a high level of activation and share a phenotypic  
70 and transcriptomic core signature across different tissues. Nevertheless, they also possess  
71 unique characteristics and functions shaped by the microenvironment of their respective  
72 residing sites. The trTregs program is established through a stepwise process, beginning with an  
73 initial commitment in peripheral lymphoid organs and culminating in final differentiation within  
74 tissues [6–8]. Regarding function, trTregs located in adipose tissue adapt to regulate metabolism  
75 and restrain obesity [9]. This cell subset also orchestrates tissue regeneration and homeostasis  
76 in the colon [10], participates in skeletal muscle (SM) regeneration and control of fibrosis  
77 [11,12], facilitates wound healing and hair growth in the skin [13,14] and promotes myelin  
78 regeneration in the central nervous system (CNS) [15]. Throughout these contexts, the survival,  
79 expansion, and acquisition of tissue-repair properties by trTregs have been demonstrated to rely  
80 on IL-33, an alarmin belonging to the IL-1 family, released upon cellular damage [16].  
81 Correspondingly, trTregs express the specific IL-33 receptor subunit, ST2 [5].  
82 The majority of studies on trTregs have focused on their behavior under homeostatic conditions  
83 or in models of sterile injury, where they accumulate locally to facilitate tissue healing [17].  
84 Nonetheless, limited information exists concerning trTregs behavior and their dependence on  
85 the IL-33/ST2 axis for controlling tissue damage induced by infections, which exposes these cells  
86 to a distinct environment. Currently, only a handful of studies have demonstrated local trTregs  
87 accumulation and their role in promoting tissue repair during acute infections caused by  
88 influenza virus [18], herpes simplex virus [19], and cytomegalovirus [20]. Intriguingly, trTregs  
89 accumulation in the lung and cornea appeared to rely more on IL-18, another IL-1 family  
90 cytokine, than on IL-33 signaling. Additionally, trTregs increased in the liver during *S. japonicum*  
91 helminth infection, where they significantly ameliorated tissue pathology [21]. In contrast, ST2+  
92 Tregs that accumulated in the intestinal lamina propria of chronically HIV-infected patients had

93 a limited role in tissue repair, as these individuals exhibited heightened epithelial permeability  
94 and tissue fibrosis [22]. In protozoan infections, different roles for trTregs have been reported,  
95 with their protective function noted in cerebral malaria [23], while their relevance in SM  
96 pathology during toxoplasmosis appeared negligible [24]. Despite these emerging reports, the  
97 role of trTregs and the IL-33/ST2 axis in tissue repair and homeostasis during infections remains  
98 poorly delineated. Few studies have examined the impact of manipulating the abundance of  
99 trTregs on antimicrobial immunity and pathogen load control. Given that trTregs are recognized  
100 for their strong suppressive potential [4,25], further exploration of their influence on effector  
101 immune responses is necessary. This exploration will contribute to a better understanding of  
102 the interplay between microbial persistence, tissue damage and repair, and the underlying  
103 immunopathology that characterizes certain chronic infections.

104 Chagas' Disease (American Trypanosomiasis) is a chronic infection caused by the protozoan  
105 parasite *Trypanosoma cruzi*. It is endemic in Latin America, but cases are also reported in non-  
106 endemic regions, with approximately 6-7 million people estimated to be infected worldwide  
107 [26]. During the acute phase, the parasite invades cells from tissues such as muscle, liver, gut,  
108 lymph nodes, spleen, and the CNS, where it actively replicates, inducing cell death and tissue  
109 damage. Consequently, the acute phase of this infection is associated with high parasitemia and  
110 nonspecific symptoms. Type 1 immunity, characterized by elevated levels of proinflammatory  
111 cytokines like IFN- $\gamma$  [27–29], along with innate and adaptive immune cells like NK cells,  
112 inflammatory macrophages, and CD8+ T lymphocytes [28,30,31], work together to minimize  
113 parasite replication and burden. However, this immune response is insufficient to completely  
114 eradicate the parasite from the host, leading to chronic infection. During the chronic phase,  
115 around 30% of infected individuals will develop specific symptoms related to digestive or cardiac  
116 pathology after 10-30 years [32]. Presently, evidence suggests that both parasite persistence  
117 and a sustained inflammatory environment mediate the characteristic tissue damage observed  
118 in this disease during the chronic phase [33]. In addition to the classical pathology, muscular

119 pain and weakness are frequently observed in both acute and chronic Chagas' patients [34–36].  
120 Furthermore, an association between SM parasitism and myositis, with structural alterations of  
121 muscular fibers, has been demonstrated in chronically infected humans [37,38], as well as in  
122 mouse models of acute and chronic infection [39–43].

123 In this study, we used a mouse model of acute *T. cruzi* infection to investigate trTregs and their  
124 association with tissue damage and protective immunity. We examined trTregs dynamics in this  
125 infection scenario, characterized by a unique combination of elevated systemic tissue injury and  
126 a limited Tregs response [44]. We found reduced trTregs numbers in target tissues that  
127 correlated with reduced systemic IL-33 levels. By supplementation with recombinant IL-33, we  
128 dissected the impact of trTregs and other IL-33-responsive immune subsets on tissue damage,  
129 parasite control, and infection progression. Through this work, we shed light on the intricate  
130 balance between microbicidal and regenerative responses driven by trTregs and the IL-33/ST2  
131 axis, an area still inadequately defined in infections and of particular relevance to the  
132 progression of acute Chagas' Disease.

133

## 134 RESULTS

### 135 **Systemic tissue damage during acute *T. cruzi* infection associates with tissue** 136 **parasitism and immune infiltrate**

137 As a first step to dissect the ability of trTregs to control damage, we initially assessed the extent  
138 and progression of tissue injury in our experimental model of acute *T. cruzi* infection. As  
139 established in our lab [45], intraperitoneal injection of 5,000 trypomastigotes (Tulahuen strain)  
140 induces a peak of parasitemia at 21 days post-infection (dpi) (Fig 1A). This is accompanied by the  
141 maximum parasite load in tissues such as SM, heart, spleen, and liver (Fig 1B), as well as the  
142 peak of immune cell expansion in the spleen (Fig 1C). In agreement with previous findings

143 [39,46], histological examination of SM at the infection peak revealed the presence of parasite  
144 nests and diffuse mononuclear infiltrate associated with necrosis and calcification of muscular  
145 fibers, absent in samples from non-infected (NI) mice (Fig 1D). Quantification of the immune  
146 infiltrate in SM showed that leucocyte counts were also at their maximum at 21 dpi (Fig 1E).

147 To further elucidate the impact of *T. cruzi* infection on muscle physiology, we conducted a  
148 whole-tissue RNAseq comparing infected (INF) versus NI quadriceps. The transcriptome analysis  
149 identified 1621 differentially expressed genes (DEGs) between both conditions. Non-supervised  
150 pathway analysis of the DEGs using EnrichR revealed that, in addition to pathways associated  
151 with immune responses such as interferon-gamma, interferon-alpha and complement  
152 responses, several pathways related to muscle physiology such as oxidative phosphorylation,  
153 myogenesis and adipogenesis were among the most significantly enriched pathways (Fig 1F). As  
154 expected, volcano plots revealed that most genes associated with the pathways linked to  
155 immune responses were upregulated by the infection (S1A Fig and S1 Table). In contrast, the  
156 majority of genes linked to muscle physiology pathways were downregulated (Fig 1G and S1  
157 Table), supporting the notion that acute infection disrupted SM homeostasis. Consistent with  
158 histological and transcriptomic evidences of SM damage, we found increased plasma activity of  
159 creatine phosphokinase (CPK) and creatine phosphokinase of muscle and brain (CPK-MB) at 21  
160 dpi compared to NI mice (Fig 1H). The alteration of additional markers of systemic damage such  
161 as increased activity of lactate dehydrogenase (LDH), glutamic oxaloacetic transaminase (GOT)  
162 and glutamic pyruvic transaminase (GPT), along with hypoglycemia, indicated affection of  
163 various target tissues beyond SM, as previously reported by our group [44,47] . As expected, the  
164 greatest tissue alteration coincides with highest parasitemia counts and tissue parasitism (Figs  
165 1A and 1B) as well as with the peak of immune cells expansion in the spleen (Fig 1C) and  
166 maximum immune infiltration in SM (Fig 1E), and other target tissues such as heart and liver  
167 (S1B Fig). Given these features, the acute phase of *T. cruzi* infection emerged as an instrumental  
168 setting to study trTregs roles during the infection.

169

170 ***Bona fide* trTregs are reduced in target tissues and lymphoid organs at the peak of**  
171 **infection**

172 Given that the greatest alteration of biochemical markers of tissue damage was observed at the  
173 peak of infection, we selected 21 dpi as the initial time point to evaluate by flow cytometry the  
174 presence of total Tregs as well as of trTregs in different *T. cruzi* target sites. As previously  
175 documented [44], *T. cruzi* infected mice exhibited reduced frequencies of total Tregs in spleen  
176 and liver around the peak of the infection (S2A and S2B Figs). An even more pronounced  
177 decrease was observed when analyzing other peripheral tissues known to be common parasite  
178 targets, such as SM and the heart. We then quantified trTregs that were identified within the  
179 Foxp3+ Tregs population according to their co-expression of ST2 and KLRG-1, as proposed by  
180 Delacher et al. [5]. We detected a notable reduction in the presence of trTregs, both in terms of  
181 frequency within total Tregs and in absolute numbers, in SM, liver and spleen from INF animals  
182 compared to NI controls (Figs 2A and 2B). This subset was not evaluated in the heart due to the  
183 remarkably low infiltration of total Tregs, which impeded a more in-depth examination of this  
184 organ.

185 Afterwards, we determined whether trTregs identified through the co-expression of ST2 and  
186 KLRG-1 in the context of the infection possessed distinctive phenotype of *bona fide* tissue repair  
187 cells, setting them apart from classic ST2- KLRG-1- lymphoid-like Tregs as previously described  
188 in other experimental settings [5,7,48–52]. Thus, we compared the expression of transcription  
189 factors (BATF, IRF4 and Ki-67) and surface molecules (CD44, CD62L, TIGIT, ICOS, GITR, PD-1 and  
190 CTLA-4), as well as amphiregulin (Areg) production by flow cytometry in trTregs and ST2- KLRG-  
191 1- Tregs from spleen of INF and NI mice identified as depicted in Fig 2A. As shown in the  
192 representative histograms from S3 Fig and summarized in the heatmap in Fig 2C, the expression  
193 levels of most evaluated markers, with the exception of CD62L, were higher in trTregs compared



194 to ST2- KLRG-1- Tregs obtained from the spleen of NI mice. Notably, trTregs from the spleen of  
195 INF mice also exhibited a *bona fide* trTregs phenotype, displaying even stronger phenotypic  
196 features in comparison to their ST2- KLRG-1- Tregs counterparts, with the highest expression of  
197 certain markers as BATF, IRF4, ICOS and GITR along with reduced CD44, TIGIT and PD1 levels. A  
198 principal component analysis (PCA) of the phenotypic data demonstrated that while ST2- KLRG-  
199 1- Tregs from spleens of NI and INF mice clustered closely, trTregs segregated apart along PC1,  
200 that explains around 70% of the variance among the samples (Fig 2D). Furthermore, trTregs from  
201 NI and INF mice showed some differences between them at expense of PC2, which explains  
202 around 20% of the variance mainly driven by CD62L expression.

203 As trTregs have been shown to increase once the tissue damage is well established [11,12,18–  
204 21], we evaluated trTregs response along the acute phase of the infection (Fig 2E). Despite  
205 observing a transient increase in trTregs numbers in the liver at 10 dpi, we found a significant  
206 reduction in the frequency and absolute number of this cell subset at 21 dpi in all evaluated  
207 tissues. It is noteworthy that while trTregs absolute numbers recover at later time points, they  
208 do not substantially increase as observed in other injury models.

209 In summary, our results indicate that during acute *T. cruzi* infection, despite the severe systemic  
210 tissue damage, trTregs are particularly reduced within an already restricted total Treg pool. The  
211 few remaining trTregs found at the peak of infection share several characteristics with *bona fide*  
212 trTregs, presenting particularities likely as a consequence of the infection.

213

#### 214 **Systemic IL-33 levels are reduced during acute *T. cruzi* infection.**

215 It is established that trTregs development is a multi-step process that initiates with a  
216 specialization commitment in secondary lymphoid organs and culminates after migration into  
217 residence tissues [6–8]. Remarkably, IL-33 has been shown to play a role in all these different

218 stages [53]. In light of the general decline in trTregs numbers despite the elevated tissue damage  
219 around the peak of acute infection, we performed a kinetic study to assess IL-33 concentrations  
220 at both systemic and peripheral sites. Our analysis revealed that plasma IL-33 concentration was  
221 detectable in NI mice and diminished during the course of acute *T. cruzi* infection, showing a  
222 statistically significant decrease at 21 dpi, followed by a return to baseline levels at 35 dpi (Fig  
223 3A). A similar trend was observed when quantifying IL-33 in the spleen homogenates (S4A Fig).  
224 In contrast, the quantification of total IL-33 in homogenates from target tissues showed an  
225 increased concentration at 21 and 35 dpi in SM (Fig 3A) while it remained relatively constant  
226 throughout the tested period in the liver (S4A Fig). These results indicate that, despite a  
227 conservation or increase in IL-33 levels in peripheral non-lymphoid tissues, its concentration is  
228 reduced at systemic level and in secondary lymphoid tissues, suggesting that the initial steps of  
229 trTregs development may be affected during *T. cruzi* infection.

230

231 **IL-33 supplementation expands trTregs from acutely infected animals *in vitro* but fails**  
232 **to prevent trTregs reduction in established infection.**

233 To investigate the possible role of trTregs in managing damage and the progression of pathology  
234 in *T. cruzi* infection, we aimed to increase trTregs numbers by administrating recombinant IL-33  
235 (rIL-33) in our experimental setting. As a proof of principle, we first evaluated the responsiveness  
236 of trTregs from INF mice to IL-33. To this end, splenic Tregs (CD4+ Foxp3-GFP+) sorted from INF  
237 mice and NI mice were stimulated with anti-CD3, anti-CD28 and rIL-2 in the presence or absence  
238 of rIL-33 (Fig 3B). The addition of IL-33 to cultures containing Tregs from INF mice resulted in an  
239 expansion of trTregs, leading to a final percentage of ST2+ KLRG-1+ Tregs comparable to that  
240 obtained in IL-33-supplemented NI Tregs cultures. Notably, IL-33 supplementation failed to  
241 induce ST2 and KLRG-1 expression in conventional T cells (CD4+ Foxp3-GFP-) obtained from the  
242 spleens of either INF or NI animals (S4B Fig). These results indicate that rIL-33 specifically acts

243 on the Tregs pool by expanding trTregs even when they are isolated from the *T. cruzi* infection  
244 environment, supporting its potential for treating INF animals.

245 For the *in vivo* treatment, with the aim of preventing the infection-induced reduction of trTregs,  
246 we administered rIL-33 (or PBS as control) intraperitoneally at 12, 15 and 18 dpi, as schematized  
247 in Fig 3C. In an alternative approach, mice were co-administered with rIL-2 and rIL-33  
248 considering the relevance of IL-2 for Tregs survival [54] and taking into account that systemic  
249 levels of this cytokine remain unchanged even after the increased cell demand resulting from T  
250 cell expansion during acute *T. cruzi* infection [44]. As a positive control of its biological activity,  
251 we observed that *in vivo* intraperitoneal (i.p.) administration of IL-33 to NI animals led to trTregs  
252 expansion (Fig 3D), as previously reported [5]. Remarkably, the treatment with rIL-33 or rIL-33  
253 plus rIL-2 in INF mice failed to increase trTregs frequency or absolute numbers in SM and spleen  
254 when compared to PBS-treated controls (Fig 3E). The injection of rIL-33 alone had effect on the  
255 liver, resulting in an increase in trTregs frequency and a subsequent recovery in trTregs absolute  
256 numbers, which reached levels similar to those observed in the livers of untreated NI mice  
257 (represented by grey dashed lines) (Fig 3E). To further address whether IL-33 supplementation  
258 had an impact on tissue damage or infection progression, despite the limited effect on trTregs,  
259 we initially examined the plasma levels of biochemical markers indicative of tissue damage. The  
260 treatment with rIL-33 did not improve these markers, while the injection of rIL-2 plus rIL-33  
261 appeared to worsen them compared to PBS-treated controls (S4C Fig). Moreover, global  
262 indicators of disease progression, such as total weight loss at the peak of infection and overall  
263 survival, also showed no differences between treated and control mice (S4D and S4E Figs).

264 Since systemic (i.p.) treatment with IL-33 in INF mice did not yield any significant effects on the  
265 evaluated parameters, we speculated that local administration in peripheral tissue may better  
266 target trTregs. Therefore, we tested the effect of intramuscular (i.m.) rIL-33 injections. In this  
267 approach, INF mice were injected at 12, 15 and 18 dpi with rIL-33 (0.3 $\mu$ g per muscle) in one hind

268 limb and with PBS in the other as control, according to the procedure described by Kuswanto et  
269 al., 2016 [12]. Similar to systemic treatment, i.m. rIL-33 injection in NI animals resulted in an  
270 accumulation of Tregs in SM, which contained a high proportion of trTregs (S4F Fig), while it had  
271 no effect on INF animals (S4G Fig).

272 Overall, these results indicate that, although trTregs from INF mice are intrinsically able to  
273 respond to IL-33, the reduction of trTregs that occurs during acute *T. cruzi* infection cannot be  
274 rescued by rIL-33 administration, likely due to particular signals generated in the context of an  
275 established infection.

276

277 **Inflammatory and microbial-derived signals are unable to restrict IL-33 mediated**  
278 **expansion of trTregs *in vitro*.**

279 To comprehend the mechanisms contributing to the limited impact of rIL-33 on inducing trTregs  
280 during *T. cruzi* infection, we directed our attention towards molecules known to counteract IL-  
281 33's biological effects, potentially activated by this parasitic infection. Specifically, we examined  
282 soluble ST2 (sST2), a spliced variant of ST2 lacking the cytosolic and transmembrane domains,  
283 which acts as a decoy receptor to neutralize IL-33 activity under various inflammatory conditions  
284 [55]. Our findings revealed undetectable levels of sST2 in the serum from both NI and INF mice  
285 (Fig 4A). Within tissues, sST2 levels were shown to be similar between INF mice and NI  
286 counterparts in spleen and SM lysates while in the liver, sST2 levels could not be quantified as  
287 they were remarkably high, surpassing the methodological higher detection point even in  
288 diluted lysates.

289 Beyond sST2, several pro-inflammatory cytokines such as IL-1 $\beta$ , IL-27, IFN- $\gamma$  and TNF have been  
290 demonstrated to prevent IL-33 effects on target cells [56–58]. Indeed, the latter two can block  
291 *in vivo* the expansion of trTregs induced by rIL-33. Given the significant increase in some of these

292 and other inflammatory signals like IL-6, IL-12 and IL-18 during acute *T. cruzi* infection [44,59,60],  
293 we explored their potential role in preventing the IL-33-mediated trTregs expansion in our  
294 experimental setting. To this end, we took advantage of the *in vitro* approach described in Fig  
295 3B. Sorted splenic Tregs from NI mice were cultured in the presence of the trTregs expansion  
296 cocktail (anti-CD3, anti-CD28 plus rIL-2 and rIL-33) along with other recombinant cytokines,  
297 conditioned media or other stimuli (Fig 4B). None of the individual cytokines tested nor a Th1  
298 differentiation cocktail (IL-12 plus anti-IL-4) were capable of preventing the expansion of trTregs  
299 induced by IL-33. We also considered that, in the context of *T. cruzi* infection, multiple  
300 inflammatory signals may concurrently exist and synergize to block IL-33's effect. Therefore, we  
301 simulated these conditions using conditioned media obtained after 24-hour of polyclonal  
302 stimulation of splenocytes obtained from NI or INF (10 and 21 dpi) mice. None of these  
303 conditioned media were able to abrogate the IL-33-induced trTregs expansion. Then, a second  
304 approach involving transwell cultures was designed to emulate the early stages of infection. In  
305 this assay, where Tregs were co-cultured in the upper transwell chamber with splenocytes of NI  
306 mice either alone or in the presence of trypomastigotes, IL-2 and IL-33 also retained their  
307 capacity to expand trTregs.

308 Finally, considering that the maximal trTregs reduction correlates with the highest parasitemia,  
309 and taking into account previous results indicating that Treg differentiation is affected by the  
310 presence of parasites [44], we further evaluated a possible inhibitory effect from microbial  
311 ligands. To this end, heat-killed or lysed trypomastigotes were added to the cultures, however,  
312 even in the presence of these sources of microbial ligands, trTregs cell expanded normally in the  
313 presence of IL-2 + IL-33 (Fig 4C).

314 Collectively, these findings suggest that the ineffectiveness of IL-33 treatment in promoting  
315 trTregs cells is not likely due to increased levels of a well-known IL-33 modulator such as sST2 or  
316 the influence of prominent inflammatory cytokines or microbial ligands heightened in the

317 context of *T. cruzi* infection. Instead, a complex combination of different signals, an unidentified  
318 modulator, or other mechanisms may underlie the absence of effect after IL-33 injection in  
319 established *T. cruzi* infection.

320

321 **Early rIL-33 administration expands trTregs and improve disease outcome in infected**  
322 **mice.**

323 In a subsequent effort to modulate the trTregs response *in vivo* during acute infection, and  
324 considering that results from the previous section suggested that IL-33 injection expands trTregs  
325 *in vivo* in NI mice but its effects are restrained by an unidentified signal(s) emerging along the  
326 infection, we opted to treat INF mice with rIL-33 on 0, 3, and 6 dpi (Fig 5A).

327 Early IL-33 injection expanded trTregs in infected (INF) mice, as evidenced by the tendency for  
328 trTreg frequency and absolute numbers to increase in SM, alongside significant increases  
329 observed in the liver and spleen by 21 dpi (Figs 5B, 5C and S5A Fig). Of note, trTregs numbers  
330 from IL-33 treated INF animals exceeded those observed in untreated NI mice (S5A Fig,  
331 represented by grey dashed lines). These results illustrated the efficiency of early IL-33  
332 treatment in sustaining elevated trTregs throughout at least the two-week period up to the peak  
333 of the infection, raising the possibility it may impact on tissue repair mechanisms and infection  
334 progression. To assess this, we measured several parameters such as biochemical markers of  
335 tissue damage, total body weight loss and SM strength (S5B-D Figs). The analysis of the outcome  
336 of these parameter evaluations revealed an overall improvement in the health state of the IL-  
337 33-treated group at 21 dpi, as summarized in the heatmap in Fig 5D. To characterize changes  
338 occurring in target tissues with IL-33 treatment, we performed histological analysis on SM. The  
339 results shown similar alterations in SM architecture between both experimental groups,  
340 characterized by the presence of a diffuse mononuclear infiltrate, necrosis and calcification of

341 muscular fibers. Additionally, all mice showed scarce number of centrally nucleated muscle cells,  
342 which are associated with tissue regeneration [61] (S5E Fig).

343 The responsiveness to IL-33 is mediated by ST2, expressed in different immune cell types [16,55].

344 Therefore, it is expected that our early IL-33 treatment during *T. cruzi* infection may affect other  
345 ST2-expressing cell subsets involved in tissue damage control such as type 2 Innate lymphoid  
346 cells (ILC2) [49,62]. Accordingly, we assessed ILC2 infiltrate in different tissues using the gating  
347 strategy shown in S5F Fig, adapted from the protocol reported by Tait Wojno and Beamer [63].  
348 As anticipated, ILC2 frequency and absolute numbers were also increased after rIL-33 injection  
349 during early *T. cruzi* infection (Figs 5E and 5F, and S5G Fig).

350 In addition to trTregs and ILC2, IL-33 can activate effector immune cells either directly through  
351 ST2 signaling on the target cell or indirectly by inducing the production of intermediate cues,  
352 such as IFN- $\gamma$  [10,55,64,65]. We, therefore, evaluated if early IL-33 administration affected  
353 parasite specific CD8<sup>+</sup> T cells, an effector response critical for *T. cruzi* control [66]. Interestingly,  
354 IL-33 treated animals showed increased frequencies of this cell subset in SM, liver as well as in  
355 spleen (Figs 5G and 5H). These changes in frequency corresponded with a tendency toward  
356 higher counts of parasite-specific CD8<sup>+</sup> T cells in SM, conserved counts in the liver, and increased  
357 counts in the spleen (S5H Fig). In correlation with these results, INF mice that received IL-33  
358 injection showed significantly decreased parasitism in non-lymphoid tissues such as SM, heart  
359 and liver (Fig 5I).

360 Altogether, these findings demonstrate that early rIL-33 administration can improve the course  
361 of acute infection, not only by reducing tissue damage, but also by increasing parasite control.  
362 These results may be attributed to the combined effect of IL-33 on different immune cell subsets  
363 such as trTregs, ILC2 and effector CD8<sup>+</sup> T cells.

364

## 365 DISCUSSION

366 Previous reports indicate that tissue injury, whether sterile or infection-derived, is associated  
367 with trTregs accumulation due to increased IL-33 release after cell destruction [16]. This  
368 reparative mechanism is well described in sterile damage, particularly within SM [4,11,12]. In  
369 the context of acute *T. cruzi* infection—a model for Chagas' disease with a profound compromise  
370 of various target tissues, including SM—our results unveil a novel scenario marked by a  
371 diminished trTregs response and reduced plasmatic IL-33 concentration despite extensive tissue  
372 damage. This suggests a specific impairment in the regulatory fate associated with tissue repair,  
373 complementing our earlier work which reported limited Tregs responses but with the acquisition  
374 of a type 1 specialization profile during *T. cruzi* infection [44]. Altogether, our findings delineate  
375 a scenario where the reduction of a reparative/regulatory cell subset during the acute phase  
376 may potentially facilitate tissue damage by compromising physiological repair mechanisms.  
377 Indeed, a detailed characterization of tissue damage associated with *T. cruzi* infection,  
378 particularly in SM, revealed a clear modification in the SM transcriptome with activation of  
379 immune-related pathways and a general downregulation of genes associated with myogenesis,  
380 adipogenesis, and oxidative phosphorylation pathways, linked to normal muscle physiology and  
381 repair processes after injury [67–69]. Therefore, our results provide evidence that during acute  
382 *T. cruzi* infection, the transcriptional landscape in SM denotes damage and correlates with a  
383 reduced frequency of trTregs. This association may potentially connect deficient repair  
384 processes with long-term consequences in chronic immunopathology during Chagas' disease.  
385 Further studies may be required to deeply assess these possible connections.

386 The attenuation of the reparative response during acute *T. cruzi* infection was systemic,  
387 manifested by reduced frequency and absolute numbers of trTregs across evaluated tissues,  
388 including SM, liver, and spleen. Unexpectedly, IL-33 levels exhibited both consistency and  
389 discrepancy: plasma IL-33 concentration diminished, correlating with the limited trTregs



390 responses, while muscle IL-33 increased, yet failed to prevent the reduction of trTregs in that  
391 tissue. Two aspects of these findings were puzzling: the unexpected reduction in systemic IL-33  
392 levels despite documented tissue damage in *T. cruzi* infection and the lack of an accompanying  
393 increase in trTregs in muscle despite an elevated local IL-33 concentration. The mechanisms  
394 regulating IL-33, which are complex and varied, include its rapid degradation after tissue injury  
395 [16,70,71]. For example, caspases 1 and 7, produced in inflammatory contexts and involved in  
396 the death of infected cells, fragment IL-33 to inactivate it [72]. Additionally, IL-33 is easily  
397 oxidizable in the extracellular space, limiting ST2-dependent immunological responses [73].  
398 Accordingly, the inflammatory milieu during acute *T. cruzi* infection could rapidly oxidize and/or  
399 degrade IL-33, diminishing its availability, especially in plasma. In contrast, elevated IL-33 levels  
400 were detected in muscle. However, this quantification was conducted in tissue lysates,  
401 presenting technical limitations that impede confirmation of the extracellular presence and,  
402 consequently, the availability of IL-33 for ST2+ cells. Discrepancies between IL-33 concentration  
403 and trTregs numbers in SM suggest potential unavailability or counteraction by inflammatory  
404 signals. Alternatively, trTregs cells may face high mortality or reduced generation during the  
405 acute stage. Considering the multi-step development of trTregs beginning in the spleen [8,74],  
406 the reduction in IL-33 levels in this organ during acute infection could be linked to a lower  
407 generation of these cells and, consequently, their reduced arrival at target organs.

408 Given the scenario described earlier, and our aim to understand the impact of trTregs reduction  
409 on disease progression, we intended to boost the numbers of this cell subset through rIL-33  
410 supplementation in established *T. cruzi* infection. However, IL-33 treatment, administered  
411 systemically or locally around the second week of infection, failed to rescue trTregs numbers  
412 and had no effect on disease progression. Notably, the lack of response to IL-33 in terms of  
413 trTregs expansion was specific to the infection condition, as this cytokine increased trTregs in  
414 non-infected animals. The ability of trTregs from infected mice to expand upon IL-33 stimulation  
415 *in vitro* suggests intrinsic responsiveness to this growth factor, pointing to a restrictive *in vivo*

416 environment imposed by the infection. As we established that inflammatory environments or  
417 even the parasite itself might negatively affect Tregs differentiation [44], and considering that  
418 inflammatory cytokines can impede IL-33 signaling in trTregs [57], we investigated potential  
419 infection-associated cues that could counteract IL-33's effect. We found that sST2, a natural  
420 decoy receptor of IL-33 signaling [55], is not increased during *T. cruzi* infection, suggesting that  
421 it is unlikely involved in the lack of response to IL-33 in our infection setting. Further evaluation  
422 through *in vitro* approaches, combining rIL-33 with various inflammatory or parasite signals,  
423 failed to identify any molecule, cocktail, or conditioned media capable of blocking IL-33-  
424 mediated expansion of trTregs. These results emphasize that the intricate combination of signals  
425 present in a living host undergoing acute *T. cruzi* infection is challenging to replicate with *in vitro*  
426 approaches, making it difficult to identify critical determinants of an environment particularly  
427 restrictive for regulatory pathways.

428 As an alternative strategy to assess IL-33 effects while avoiding the restrictive environment  
429 around the peak of *T. cruzi* infection, we implemented early treatment during the first week of  
430 infection. This approach resulted in a less severe acute infection progression along with better  
431 parasite control. Given that IL-33 is able to modulate several immune cell subsets [70], we  
432 focused not only on trTregs but also on ILC2 and CD8+ T cells. Early IL-33 supplementation during  
433 *T. cruzi* infection led to a significant expansion of trTregs, consistent with previous reports  
434 [12,20,24]. Notably, the magnitude of the trTregs response increased not only in secondary  
435 lymphoid organs such as the spleen but also in target organs like the liver and SM, remaining  
436 evident even at the infection's peak. Interestingly, early IL-33 treatment also elevated ILC2 and  
437 parasite-specific CD8+ T cell frequencies. ILC2 play crucial roles in combating certain infectious  
438 agents and, similar to trTregs, promote tissue reparative processes [62]. Indeed, IL-33-mediated  
439 ILC2 expansion has been linked to infection resistance against cerebral malaria and various  
440 intestinal infections [23,75–77]. Moreover, our comprehensive evaluation of immune cell  
441 subsets highlighted that IL-33 potentiated antiparasitic CD8+ T cell immunity, aligning with

442 previous research that suggested a role for this alarmin in inducing robust antiviral responses  
443 [78,79]. In particular, IL-33 has been recently shown to preserve CD8+ T cell stemness and re-  
444 expansion capacity in the context of a chronic viral infection [80].

445 In summary, our findings underscore the positive impact of IL-33 supplementation during early  
446 *T. cruzi* infection, contributing to reduced tissue damage and improved parasite control. Building  
447 upon existing research, we propose that this beneficial effect arises from the concerted action  
448 of expanding cell subsets involved in tissue repair, such as trTregs and ILC2, alongside those  
449 engaged in microbial control, particularly CD8+ T cells. Future studies are warranted to  
450 meticulously dissect the specific roles of each of these immune cell subsets in mediating the  
451 effects of IL-33 on *T. cruzi* infection outcome. Interestingly, the simultaneous expansion of  
452 trTregs and parasite-specific CD8+ T cells might seem counterintuitive, given numerous reports  
453 linking regulatory responses with diminished antimicrobial immunity [81]. Our previous study in  
454 the context of *T. cruzi* infection demonstrated that adoptive Tregs transfer represses parasite-  
455 specific CD8+ T cell responses [44]. Furthermore, it has been shown that tissue resident Tregs  
456 exhibit heightened regulatory features [25]. Significantly, our results challenge this notion by  
457 revealing that boosting specialized regulatory T cell responses does not necessarily attenuate  
458 effector responses. This simultaneous enhancement of both regulatory/reparative and  
459 antiparasitic cell subsets, likely a result of the individual effects of IL-33 on each ST2-expressing  
460 subset, proves to be beneficial for the progression of acute *T. cruzi* infection. This discovery  
461 establishes a precedent, suggesting the potential for rational novel therapies in Chagas' Disease  
462 or other infectious diseases. To date, only one study has evaluated IL-33 expression in chronic  
463 Chagas disease patients showing no correlation with disease severity [82]. Therapies involving  
464 IL-33 could be designed to modulate the immune system, favoring a specific combination of  
465 regulatory and effector responses. The goal would be to enable effective pathogen clearance  
466 while minimizing collateral damage, thereby preventing clinical pathology.

467

## 468 MATERIALS AND METHODS

### 469 **Ethics statement**

470 Mouse handling followed international ethical guidelines. All experimental procedures were  
471 conducted in compliance with the ethical standards set by the Institutional Animal Care and Use  
472 Committee of Facultad de Ciencias Químicas – Universidad Nacional de Córdoba, and were  
473 approved under protocol numbers RD-733-2018.

474

### 475 **Mice.**

476 Age-matched (8 to 12 week-old) mice of both sexes were used. Foxp3-GFP reporter mice (B6.Cg-  
477 Foxp3tm2Tch/J) were obtained from The Jackson Laboratories (USA). BALB/c mice were  
478 obtained from School of Veterinary, La Plata National University (La Plata, Argentina). Animals  
479 were bred in the animal facility of the Facultad de Ciencias Químicas, Universidad Nacional de  
480 Córdoba, and housed under a 12:12 h light-dark cycle with food and water ad libitum. The  
481 institutional animal facility follows the recommendations of the Guide for the Care and Use of  
482 Experimental Animals, published by the Canadian Council for the Protection of Animals.

483

### 484 **Parasites and experimental infection.**

485 For all experiments, *T. cruzi* Tulahuén strain was used. Bloodstream trypomastigotes were  
486 maintained in male BALB/c mice by serial passages every 10-11 days. For *in vivo* assays, Foxp3-  
487 GFP reporter mice were inoculated intraperitoneally with 0.2 mL PBS containing 5000  
488 trypomastigotes.

489 For *in vitro* assays, trypomastigotes were obtained from the extracellular medium of infected  
490 monolayers of Vero cells cultured in RPMI 1640 medium (Gibco, Invitrogen) containing 10% heat  
491 inactivated fetal bovine serum (FBS, Natocor), 2 mM glutamine (Gibco), 10 mM HEPES (Gibco)  
492 and 40 ug/mL gentamicin (Veinfa Laboratories). After 7 days of infection, extracellular medium  
493 was collected, centrifuged at 1800 g for 30 min at room temperature and incubated for 2 h at  
494 37 °C. Trypomastigotes were recovered from the supernatant and counted using a Neubauer  
495 chamber. Heat-killed trypomastigotes were obtained after incubation at 56 °C for 10 min  
496 (adapted from [83]), while lysed trypomastigotes were obtained after 3 cycles of freeze/thaw  
497 and 5 minutes of sonication (adapted from [84]).

498

#### 499 **Parasite quantification in blood and tissues.**

500 Parasitemia was monitored by counting the number of viable trypomastigotes in blood after  
501 lysis with a 0.87% ammonium chloride buffer. For tissue parasite quantification, genomic DNA  
502 was purified from 50 µg of tissue (spleen, liver, SM and heart) using TRIzol Reagent (Life  
503 Technologies) following manufacturer's instructions. Satellite DNA from *T. cruzi* (GenBank  
504 AY520036) was quantified by real time PCR using specific Custom Taqman Gene Expression  
505 Assay (Applied Biosystem) using the primer and probe sequences described by Piron et al. [85].  
506 The samples were subjected to 45 PCR cycles in a thermocycler StepOnePlus Real-Time PCR  
507 System (Applied Biosystems). Abundance of satellite DNA from *T. cruzi* was normalized to the  
508 abundance of GAPDH (Taqman Rodent GAPDH Control Reagent, Applied Biosystem), quantified  
509 through the comparative CT method and expressed as arbitrary units, as previously reported  
510 [44,47,86].

511

#### 512 **Cell preparation.**

513 To obtain cell suspensions from solid tissues, euthanized mice were perfused with 10 mL cold  
514 Hanks' Balanced Salt Solution (Gibco). Spleens and livers were obtained and mashed through a  
515 tissue strainer. Liver infiltrating cells were obtained after 25 min centrifugation (600 g without  
516 brake) in a 35% and 67.5% bilayer Percoll (GE Healthcare) gradient. The interphase containing  
517 leukocytes was recovered and washed. Erythrocytes in spleen and liver cell suspensions were  
518 lysed for 3 min in ACK Lysing Buffer (Gibco). Heart and SM (quadriceps, gastrocnemius and  
519 tibialis anterior) were excised, minced and digested for 30 min in collagenase D (2 mg/mL,  
520 Roche) and DNase I (100 µg/mL, Sigma). Digested tissues were filtered through a 70 µm filter  
521 and washed. Infiltrating leucocytes were obtained after 25 min centrifugation (600 g without  
522 brake) in a 40% and 75% bilayer Percoll gradient. The interphase was recovered and washed.  
523 Cell numbers were counted in Turk's solution using a Neubauer chamber.

524

#### 525 ***In vitro* assays**

526 For Tregs and Tconv culture, cells were purified from NI or 21 dpi Foxp3-GFP mice. CD4<sup>+</sup> cells  
527 were isolated from pooled splenic suspensions by magnetic negative selection using EasySep  
528 Mouse CD4<sup>+</sup> T Cell Isolation Kit (StemCell Technologies) according to manufacturer's instruction.  
529 Afterwards, the enriched CD4<sup>+</sup> T cell suspension was surface stained and Tregs and Tconv were  
530 further purified by cell sorting with a FACS Aria II (BD Biosciences) according to the following  
531 phenotype: Tregs (CD4<sup>+</sup> Foxp3-GFP<sup>+</sup>) and Tconv (CD4<sup>+</sup> Foxp3-GFP<sup>-</sup>). Purified cells (75000  
532 cells/well) were cultured for 3 days in 96-well U bottom plates coated with 2 µg/mL anti-CD3  
533 (eBioscience) and 1 µg/mL anti-CD28 (eBioscience) supplemented with 10ng/mL of recombinant  
534 mIL-2 (Biolegend) to allow Treg survival. Cells were cultured in complete culture media  
535 containing RPMI 1640 medium (Gibco, Invitrogen) 10% heat inactivated FBS (Natocor), 2mM  
536 glutamine (Gibco, Invitrogen), 55uM 2- mercaptoethanol (Gibco, Invitrogen) and 80ug/mL  
537 gentamicin (Veinfar Laboratories). When indicated, media contained 50 ng/mL recombinant

538 mL-33 (R&D) alone or combined with the following murine recombinant cytokines: IFN- $\gamma$  (50  
539 ng/mL, Immunotools), TNF (50 ng/mL, Immunotools), IL-1 $\beta$  (2 ng/mL, R&D), IL-6 (20 ng/mL,  
540 Shenandoah), IL-12p70 (10 ng/mL, Peprotech), IL-18 (50 ng/mL, R&D), IL-27 (20 ng/mL, R&D) as  
541 well as with 2  $\mu$ g/mL anti-mouse IL-4 (Peprotech). Alternatively, 50  $\mu$ L of conditioned media was  
542 used.

543 In co-culture transwell experiments, Tregs from NI mice were placed in the bottom of the culture  
544 plate in the presence of recombinant mL-33 and splenocytes (1:1 ratio) alone or with  
545 trypomastigotes (1:10 ratio) that were placed in the transwell chamber.

546 In co-cultures with parasite ligands, Tregs from NI animals were incubated with heat-killed or  
547 lysed trypomastigotes (ratio 1:1) in the presence of recombinant mL-33.

548

#### 549 **Conditioned media generation**

550 For conditioned media, total splenocytes were isolated from pooled splenic suspensions of NI,  
551 10 dpi and 21 dpi Foxp3-GFP mice. Cell suspensions ( $5 \times 10^6$  cells/ml) were cultured for 24 h in  
552 24-well plates in complete culture media supplemented with 50 ng/mL PMA and 1  $\mu$ g/mL  
553 ionomycin (Sigma-Aldrich).

554

#### 555 **Biochemical determinations**

556 Plasma was collected after blood centrifugation for 8 min at 3000rpm. Quantification of  
557 biochemical markers of tissue damage was performed at Laboratorio Biocon (Córdoba,  
558 Argentina) using a Dimension RXL Siemens analyzer. GOT, GPT, LDH and CPK activity was  
559 determined by UV kinetic method, CPK-MB activity was evaluated by enzymatic method, while  
560 glucose concentration was assessed by kinetic/colorimetric method.

561

### 562 **IL-33 and sST2 quantification**

563 IL-33 concentration was determined with an IL-33 Mouse ELISA kit (eBioscience), while sST2 was  
564 quantified using a Mouse ST2/IL-33R DuoSet ELISA kit (R&D Systems) in plasma and tissue  
565 lysates. Plasma samples were obtained as previously described. Tissue lysates were obtained  
566 after centrifugation at 10000g during 10 min of tissue samples homogenized in PBS containing  
567 0,5% BSA, 0,4 M NaCl, 1 mM EDTA, 0,05% Tween 20 and a protease inhibitor cocktail (Sigma-  
568 Aldrich) (adapted from [87]). GraphPad Prism 8.0.1 software was used to generate the  
569 calibration curve and determine IL-33 and sST2 concentration. In tissue lysates, values were  
570 normalized to total protein content determined using Bradford reagent (BioRad). Two Synergy  
571 HT Multi-mode microplate reader (Biotek) was used to determine absorbances at 450 nm (ELISA)  
572 and 595 nm (protein quantification).

573

### 574 **Flow cytometry**

575 Combinations of the following antibodies were used for flow cytometry: biotin polyclonal anti-  
576 Amphiregulin (R&D Systems), PE anti-BATF clone S39-1060 (BD Pharmingen), Super Bright 645  
577 anti-CD11b clone M1/70 (eBioscience), PE-Cyanine7 anti-CD11c clone N418 (eBioscience), PE  
578 anti CD127 clone A7R34 (eBioscience), PE-Cyanine7 anti-CD19 clone eBio1D3 (eBioscience), PE-  
579 Cyanine7 anti-CD3 clone 145-2C11 (eBioscience), APC, Super Bright 645 and APC-eFluor 780  
580 anti-CD4 clone GK1.5 (eBioscience), PE-Cyanine5 anti-CD44 clone IM7 (eBioscience), Alexa Fluor  
581 700 and APC-Cyanine7 anti-CD45 clone 30-F11 (eBioscience and BD Pharmingen respectively),  
582 APC-eFluor 780 anti-CD62L clone MEL-14 (eBioscience), PE-Cyanine5.5 anti-CD8 clone 53-6.7  
583 (eBioscience), Brilliant Violet 605 anti CTLA-4 clone UC10-4B9 (Biolegend), FITC anti-Foxp3 clone  
584 FJK-16s (eBioscience), Super Bright 600 anti-GITR clone DTA-1 (eBioscience), PerCp-eFluor 710  
585 anti-ICOS clone 7E.17G9 (eBioscience), PerCp-eFluor 710 anti-IRF4 clone 3E4 (eBioscience),



586 eFluor 660 anti-Ki-67 clone SolA15 (eBioscience), PE-eFluor 610 anti-KLRG-1 clone 2F1  
587 (eBioscience), PE-Cyanine7 anti-NK1.1 clone PK136 (Biolegend), Brilliant Violet 421 anti-PD-1  
588 clone 29F.1A12 (Biolegend), PE and Brilliant Violet 421 anti-ST2 clone DIH9 (Biolegend) and  
589 PerCp-eFluor 710 anti-TIGIT (eBioscience). To detect biotinylated antibodies, Streptavidin Qdot  
590 605 (Invitrogen) was used.

591 For surface staining, cell suspensions were incubated with fluorochrome labeled-antibodies  
592 together with LIVE/DEAD Fixable Aqua Dead Cell Stain Kit, for 405 nm excitation (Invitrogen) in  
593 PBS 2% FBS for 20 min at 4°C. To identify *T. cruzi* specific CD8+ T cells, cell suspensions were  
594 incubated with an H-2Kb *T. cruzi* trans-sialidase amino acids 569-576 ANYKFTLV (TSKB20) APC-  
595 or Brilliant Violet 421- labeled Tetramer (NIH Tetramer Core Facility) for 20 min at 4 °C, in  
596 addition to the surface staining antibodies.

597 For transcription factors detection, cells were initially stained for surface markers, washed, fixed,  
598 permeabilized and stained with Foxp3/Transcription Factor Staining Buffers (eBioscience)  
599 according to eBioscience One-step protocol for intracellular (nuclear) proteins. For intracellular  
600 cytokine detection,  $2 \times 10^6$  cells per well were cultured in 200  $\mu$ L supplemented RPMI 1640  
601 medium and stimulated during 2 h at 37 °C with 50 ng/mL PMA and 1  $\mu$ g/mL ionomycin (Sigma-  
602 Aldrich) in the presence of Brefeldin A and Monensin (eBioscience). Then, stimulated cells were  
603 surface-stained as indicated above, fixed and permeabilized with Intracellular Fixation &  
604 Permeabilization Buffer Set (eBioscience) or IC Fixation Buffer and permeabilization Buffer  
605 (eBioscience) following manufacturers' indications. In all cases, intracellular staining was  
606 performed by a 30 min incubation at room temperature.

607 All samples were acquired on FACSCanto II (BD Biosciences), LSRFortessa (BD Biosciences) or  
608 Attune-NxT (Life Technologies) and data were analyzed with FlowJo software version X.0.7. For  
609 cell sorting, FACS Aria II (BD Biosciences) was used.

610

## 611 **RNA sequencing**

612 Perfused mouse quadriceps were obtained and stored in RNAlater Stabilization Solution  
613 (Invitrogen) at -80°C. Then, 25mg of tissue was dissociated using Bead Ruptor Elite (Omni  
614 International) for 45 seconds at 4.85m/s and RNA was isolated using RNeasy Fibrous Tissue Mini  
615 Kit 50 (Qiagen) following manufacturer's indications. RNA concentration was determined with a  
616 Qubit 2.0 Fluorometer (Invitrogen), while a 2100 Bioanalyzer (Agilent) was used for quality  
617 evaluation. Poly(A) mRNA Magnetic Isolation Module (New England BioLabs) was used for cDNA  
618 library preparation according to manufacturer's protocol. Quality control of libraries was  
619 determined as described for RNA. Quantification of cDNA libraries was performed with PerfeCTa  
620 NGS Quantification Kit for Illumina Sequencing Platforms (QuantaBio). For each experimental  
621 group, 3 biological replicates were sequenced with NextSeq 550 (Illumina). For data analysis, a  
622 Salmon index was built from Gencode [88] Mouse release M27 (GRCm39) [GENCODE - Mouse  
623 Release M27 (gencodegenes.org)] using Salmon [89] v1.5.1 [Release Salmon 1.5.1 · COMBINE-  
624 lab/salmon · GitHub] with default k-mer size (31) and the --gencode flag. FASTQ sequence reads  
625 (SRA accession PRJNA941341) were mapped to the M27 index and transcript abundances were  
626 estimated using salmon quant on 8 threads. Salmon quant files were subsequently loaded into  
627 R v4.1.0 using tximeta v1.10.0, and differentially expressed genes were called using default  
628 parameters in DESeq2 v1.32.0 per the Bioconductor vignette [Analyzing RNA-seq data with  
629 DESeq2 (bioconductor.org)]. Genes with adjusted p-values  $\leq 0.05$  and  $|\log_2 \text{fold-change}| \geq 1$   
630 were considered differentially-expressed and included in downstream analysis. For gene set  
631 enrichment analysis, EnrichR tool [90–92] was used and MSigDB Hallmark 2020 gene sets were  
632 interrogated. Volcano plots were generated using “ggplot2” package in R. The datasets  
633 generated for this study can be found in the NIH repository under accession number  
634 PRJNA941341 (<https://www.ncbi.nlm.nih.gov/sra/PRJNA941341>).

635

### 636 ***In vivo* rIL-33 and rIL-2 treatment**

637 Recombinant mL-33 (Shenandoah) was administered via i.p. (2 µg in a total volume of 200 µL)  
638 or i.m. (0.3 µg/muscle in a total volume of 30-50 µL) at the specified time points. Dose and  
639 frequency of injections were adapted from reported protocols [12,20,24]. For i.m. treatment,  
640 quadriceps, gastrocnemius and tibialis anterior from the same hindlimb received each the dose  
641 detailed above. When indicated, i.p. injections also contained 1 µg of recombinant murine IL-2  
642 (Gibco). PBS was used as vehicle.

643

### 644 **Muscle strength and body weight evaluation**

645 Muscle strength was assessed by Kondziela's inverted screen test (hang test) [93]. Mice were  
646 kept in the experimental room for 20 minutes before the test to ensure proper adaptation to  
647 the environment. Each mouse was placed in the center of a 43 cm<sup>2</sup> wire mesh consisting of 12  
648 mm squares of 1 mm diameter wire and surrounded by a 4 cm deep wooden frame. Screen was  
649 inverted and time was measured until the mouse fell off. Maximum test duration was 2 minutes.  
650 Total body weight was determined using a precision laboratory balance.

651

### 652 **Histological analysis**

653 Perfused mouse quadriceps were fixed in formaldehyde solution and embedded in paraffin. Five  
654 µm thick sections were stained with activated hematoxylin followed by eosin alcoholic solution.  
655 Histopathological evaluation was performed by a pathologist under light microscopy.  
656 Photographs were taken using a Nikon Eclipse TE 2000 U equipped with a digital video camera.

657

### 658 **Statistics and graph creation**

659 Unless otherwise indicated, both statistics calculation and graphs creation were performed with  
660 GraphPad Prism 8.0.1 software. The normality of data distribution was assessed using Shapiro-  
661 Wilk normality test. Statistical significance of mean value comparisons was determined using t-  
662 test or One-way ANOVA for normally distributed data, and Mann-Whitney test or Kruskal-Wallis  
663 test for non-normally distributed data, as appropriate. P values  $\leq 0.05$  were considered  
664 statistically significant and are indicated in the graphs. Outliers were identified using the ROUT  
665 method. Data are presented as mean  $\pm$  SEM and the number of animals of each experimental  
666 group is indicated in the figure legends or shown in the plots. Principal Component Analysis  
667 graph and volcano plots were generated using “ggplot2” package in R software. Flow cytometry  
668 plots were exported from FlowJo software version X.0.7 after data analysis.

669

#### 670 **AI Language Model Assistance**

671 We used ChatGPT (developed by OpenAI) to assist in refining the written content of this study.  
672 ChatGPT provided suggestions and corrections based on the input provided by the user,  
673 enhancing the clarity and grammar of the text. ChatGPT output was critically revised by the user  
674 to ensure it conveys the desired message

675

#### 676 **ACKNOWLEDGMENTS**

677 We thank M. P. Abadie, M. P. Crespo, V. Blanco, D. Lutti, C. Noriega, F. A. Frontera, S. R. Oms, R.  
678 E. Villarreal, G. Furlán, N. M. Maldonado, A. Romero, L. V. Gatica and M. S. Miró (Centro de  
679 Investigaciones en Bioquímica Clínica e Inmunología) for their excellent technical assistance. We  
680 acknowledge the NIH Tetramer Core Facility for provision of APC- and Brilliant Violet 421-labeled  
681 TSKB20 tetramers. We thank S. Sandrone (Hospital Rawson, Córdoba, Argentina) for her  
682 professional commitment regarding histopathological analysis. We are also grateful to S. B.

683 Lakshminarayana, C. Osborn, D. Kristen, D. Patra for technical assistance and J. Spector  
684 (BioMedical Research, Novartis, United States) for coordinating the global health fellowship.  
685

## 686 AUTHOR CONTRIBUTIONS

687 **Conceptualization:** Eva V. Acosta Rodríguez.

688 **Formal Analysis:** Santiago Boccardo.

689 **Funding Acquisition:** Eva V. Acosta Rodríguez.

690 **Investigation:** All experimental procedures but RNAseq: Santiago Boccardo (sample collection  
691 and processing and data analysis), Constanza Rodriguez, Cintia L. Araujo Furlan, Carolina P.  
692 Abrate, Laura Almada, Camila M. S. Giménez (sample collection and processing).

693 RNAseq study: Santiago Boccardo and Manuel A. Saldivia Concepción (sample collection and  
694 processing), Peter Skewes-Cox (data compilation), Srinivasa P. S. Rao (supervision and funding).

695 **Methodology:** Santiago Boccardo, Eva V. Acosta Rodríguez.

696 **Project Administration:** Eva V. Acosta Rodríguez, Adriana Gruppi, Carolina L. Montes.

697 **Resources:** Eva V. Acosta Rodríguez, Adriana Gruppi, Carolina L. Montes, Srinivasa P. S. Rao.

698 **Supervision:** Eva V. Acosta Rodríguez.

699 **Validation:** Santiago Boccardo, Eva V Acosta Rodríguez.

700 **Visualization:** Santiago Boccardo.

701 **Writing – Original Draft Preparation:** Santiago Boccardo, Eva V Acosta Rodríguez.

702 **Writing – Review & Editing:** Adriana Gruppi, Carolina L Montes, Constanza Rodriguez, Cintia L.  
703 Araujo Furlan, Carolina P. Abrate, Laura Almada, Camila M. S. Giménez, Manuel A. Saldivia  
704 Concepción, Peter Skewes-Cox, Srinivasa P. S. Rao.

705

## 706 REFERENCES

- 707 1. Zhao H, Liao X, Kang Y. Tregs: Where We Are and What Comes Next? *Front Immunol.*  
708 2017;8: 1578. doi:10.3389/fimmu.2017.01578
- 709 2. Sakaguchi S, Mikami N, Wing JB, Tanaka A, Ichiyama K, Ohkura N. Regulatory T Cells and  
710 Human Disease. *Annu Rev Immunol.* 2020;38: 541–566. doi:10.1146/annurev-immunol-  
711 042718-041717
- 712 3. Cretney E, Kallies A, Nutt SL. Differentiation and function of Foxp3(+) effector regulatory  
713 T cells. *Trends Immunol.* 2013;34: 74–80. doi:10.1016/j.it.2012.11.002
- 714 4. Panduro M, Benoist C, Mathis D. Tissue Tregs. *Annu Rev Immunol.* 2016;34: 609–633.  
715 doi:10.1146/annurev-immunol-032712-095948
- 716 5. Delacher M, Imbusch CD, Weichenhan D, Breiling A, Hotz-Wagenblatt A, Träger U, et al.  
717 Genome-wide DNA-methylation landscape defines specialization of regulatory T cells in  
718 tissues. *Nat Immunol.* 2017;18: 1160–1172. doi:10.1038/ni.3799
- 719 6. Cho J, Kuswanto W, Benoist C, Mathis D. T cell receptor specificity drives accumulation of  
720 a reparative population of regulatory T cells within acutely injured skeletal muscle. *Proc*  
721 *Natl Acad Sci U S A.* 2019; 201914848. doi:10.1073/pnas.1914848116
- 722 7. Delacher M, Imbusch CD, Hotz-Wagenblatt A, Mallm J-P, Bauer K, Simon M, et al.  
723 Precursors for Nonlymphoid-Tissue Treg Cells Reside in Secondary Lymphoid Organs and  
724 Are Programmed by the Transcription Factor BATF. *Immunity.* 2020;52: 295-312.e11.  
725 doi:10.1016/j.immuni.2019.12.002
- 726 8. Li C, DiSpirito JR, Zemmour D, Spallanzani RG, Kuswanto W, Benoist C, et al. TCR  
727 Transgenic Mice Reveal Stepwise, Multi-site Acquisition of the Distinctive Fat-Treg  
728 Phenotype. *Cell.* 2018;174: 285-299.e12. doi:10.1016/j.cell.2018.05.004
- 729 9. Cipolletta D, Feuerer M, Li A, Kamei N, Lee J, Shoelson SE, et al. PPAR- $\gamma$  is a major driver  
730 of the accumulation and phenotype of adipose tissue Treg cells. *Nature.* 2012;486: 549–  
731 553. doi:10.1038/nature11132
- 732 10. Schiering C, Krausgruber T, Chomka A, Fröhlich A, Adelmann K, Wohlfert EA, et al. The  
733 alarmin IL-33 promotes regulatory T-cell function in the intestine. *Nature.* 2014;513:  
734 564–568. doi:10.1038/nature13577
- 735 11. Burzyn D, Kuswanto W, Kolodin D, Shadrach JL, Cerletti M, Jang Y, et al. A special  
736 population of regulatory T cells potentiates muscle repair. *Cell.* 2013;155: 1282–1295.  
737 doi:10.1016/j.cell.2013.10.054
- 738 12. Kuswanto W, Burzyn D, Panduro M, Wang KK, Jang YC, Wagers AJ, et al. Poor Repair of  
739 Skeletal Muscle in Aging Mice Reflects a Defect in Local, Interleukin-33-Dependent  
740 Accumulation of Regulatory T Cells. *Immunity.* 2016;44: 355–367.  
741 doi:10.1016/j.immuni.2016.01.009
- 742 13. Ali N, Zirak B, Rodriguez RS, Pauli ML, Truong H-A, Lai K, et al. Regulatory T Cells in Skin  
743 Facilitate Epithelial Stem Cell Differentiation. *Cell.* 2017;169: 1119-1129.e11.  
744 doi:10.1016/j.cell.2017.05.002

- 745 14. Nosbaum A, Prevel N, Truong H-A, Mehta P, Ettinger M, Scharschmidt TC, et al. Cutting  
746 Edge: Regulatory T Cells Facilitate Cutaneous Wound Healing. *J Immunol.* 2016;196:  
747 2010–2014. doi:10.4049/jimmunol.1502139
- 748 15. Dombrowski Y, O’Hagan T, Dittmer M, Penalva R, Mayoral SR, Bankhead P, et al.  
749 Regulatory T cells promote myelin regeneration in the central nervous system. *Nat*  
750 *Neurosci.* 2017;20: 674–680. doi:10.1038/nn.4528
- 751 16. Cayrol C, Girard J-P. Interleukin-33 (IL-33): A nuclear cytokine from the IL-1 family.  
752 *Immunol Rev.* 2018;281: 154–168. doi:10.1111/imr.12619
- 753 17. Astarita JL, Dominguez CX, Tan C, Guillen J, Pauli ML, Labastida R, et al. Treg  
754 specialization and functions beyond immune suppression. *Clin Exp Immunol.* 2023;211:  
755 176–183. doi:10.1093/cei/uxac123
- 756 18. Arpaia N, Green JA, Molledo B, Arvey A, Hemmers S, Yuan S, et al. A Distinct Function of  
757 Regulatory T Cells in Tissue Protection. *Cell.* 2015;162: 1078–1089.  
758 doi:10.1016/j.cell.2015.08.021
- 759 19. Varanasi SK, Rajasagi N, Jaggi U, Rouse B. Role of IL-18 induced Amphiregulin expression  
760 on virus induced ocular lesions. *Mucosal Immunol.* 2018;11: 1705–1715.  
761 doi:10.1038/s41385-018-0058-8
- 762 20. Popovic B, Golemac M, Podlech J, Zeleznjak J, Bilic-Zulle L, Lukic ML, et al. IL-33/ST2  
763 pathway drives regulatory T cell dependent suppression of liver damage upon  
764 cytomegalovirus infection. *PLoS Pathog.* 2017;13: e1006345.  
765 doi:10.1371/journal.ppat.1006345
- 766 21. Bai Y, Guan F, Zhu F, Jiang C, Xu X, Zheng F, et al. IL-33/ST2 Axis Deficiency Exacerbates  
767 Hepatic Pathology by Regulating Treg and Th17 Cells in Murine Schistosomiasis Japonica.  
768 *J Inflamm Res.* 2021;14: 5981–5998. doi:10.2147/JIR.S336404
- 769 22. Tariq M, Gallien S, Surenaud M, Wiedemann A, Jean-Louis F, Lacabaratz C, et al. Profound  
770 Defect of Amphiregulin Secretion by Regulatory T Cells in the Gut of HIV-Treated  
771 Patients. *J Immunol.* 2022;208: 2300–2308. doi:10.4049/jimmunol.2100725
- 772 23. Besnard A-G, Guabiraba R, Niedbala W, Palomo J, Reverchon F, Shaw TN, et al. IL-33-  
773 mediated protection against experimental cerebral malaria is linked to induction of type  
774 2 innate lymphoid cells, M2 macrophages and regulatory T cells. *PLoS Pathog.* 2015;11:  
775 e1004607. doi:10.1371/journal.ppat.1004607
- 776 24. Jin RM, Warunek J, Wohlfert EA. Therapeutic administration of IL-10 and amphiregulin  
777 alleviates chronic skeletal muscle inflammation and damage induced by infection.  
778 *Immunohorizons.* 2018;2: 142–154. doi:10.4049/immunohorizons.1800024
- 779 25. Matta BM, Lott JM, Mathews LR, Liu Q, Rosborough BR, Blazar BR, et al. IL-33 is an  
780 unconventional Alarmin that stimulates IL-2 secretion by dendritic cells to selectively  
781 expand IL-33R/ST2+ regulatory T cells. *J Immunol.* 2014;193: 4010–4020.  
782 doi:10.4049/jimmunol.1400481
- 783 26. World Health Organization. Chagas disease. 13 Apr 2022 [cited 14 Jun 2022]. Available:  
784 [https://www.who.int/news-room/fact-sheets/detail/chagas-disease-\(american-](https://www.who.int/news-room/fact-sheets/detail/chagas-disease-(american-trypansomiasis))  
785 [trypanosomiasis\)](https://www.who.int/news-room/fact-sheets/detail/chagas-disease-(american-trypansomiasis))

- 786 27. Abrahamsohn IA, Coffman RL. Trypanosoma cruzi: IL-10, TNF, IFN-gamma, and IL-12  
787 regulate innate and acquired immunity to infection. *Exp Parasitol.* 1996;84: 231–244.  
788 doi:10.1006/expr.1996.0109
- 789 28. Brener Z, Gazzinelli RT. Immunological control of Trypanosoma cruzi infection and  
790 pathogenesis of Chagas' disease. *Int Arch Allergy Immunol.* 1997;114: 103–110.  
791 doi:10.1159/000237653
- 792 29. Golden JM, Tarleton RL. Trypanosoma cruzi: cytokine effects on macrophage  
793 trypanocidal activity. *Exp Parasitol.* 1991;72: 391–402. doi:10.1016/0014-4894(91)90085-  
794 b
- 795 30. Padilla AM, Bustamante JM, Tarleton RL. CD8+ T cells in Trypanosoma cruzi infection.  
796 *Curr Opin Immunol.* 2009;21: 385–390. doi:10.1016/j.coi.2009.07.006
- 797 31. Tarleton RL. Depletion of CD8+ T cells increases susceptibility and reverses vaccine-  
798 induced immunity in mice infected with Trypanosoma cruzi. *J Immunol.* 1990;144: 717–  
799 724.
- 800 32. Guarner J. Chagas disease as example of a reemerging parasite. *Semin Diagn Pathol.*  
801 2019;36: 164–169. doi:10.1053/j.semmp.2019.04.008
- 802 33. Lewis MD, Kelly JM. Putting Infection Dynamics at the Heart of Chagas Disease. *Trends*  
803 *Parasitol.* 2016;32: 899–911. doi:10.1016/j.pt.2016.08.009
- 804 34. de Carvalho JF, Lerner A. Fibromyalgia associated with Chagas' disease treated with  
805 nutraceuticals. *Clin Nutr ESPEN.* 2021;42: 212–214. doi:10.1016/j.clnesp.2021.01.037
- 806 35. Köberle F. Chagas' disease and Chagas' syndromes: the pathology of American  
807 trypanosomiasis. *Adv Parasitol.* 1968;6: 63–116. doi:10.1016/s0065-308x(08)60472-8
- 808 36. Rincón-Acevedo CY, Parada-García AS, Olivera MJ, Torres-Torres F, Zuleta-Dueñas LP,  
809 Hernández C, et al. Clinical and Epidemiological Characterization of Acute Chagas Disease  
810 in Casanare, Eastern Colombia, 2012-2020. *Front Med (Lausanne).* 2021;8: 681635.  
811 doi:10.3389/fmed.2021.681635
- 812 37. Cossermelli W, Friedman H, Pastor EH, Nobre MR, Manzione A, Camargo ME, et al.  
813 Polymyositis in Chagas's disease. *Ann Rheum Dis.* 1978;37: 277–280.  
814 doi:10.1136/ard.37.3.277
- 815 38. Laguens RP, Cossio PM, Diez C, Segal A, Vasquez C, Kreutzer E, et al. Immunopathologic  
816 and morphologic studies of skeletal muscle in Chagas' disease. *Am J Pathol.* 1975;80:  
817 153–162.
- 818 39. Buckner FS, Wilson AJ, Van Voorhis WC. Detection of live Trypanosoma cruzi in tissues of  
819 infected mice by using histochemical stain for beta-galactosidase. *Infect Immun.* 1999;67:  
820 403–409. doi:10.1128/IAI.67.1.403-409.1999
- 821 40. Mendonça AAS, Gonçalves-Santos E, Souza-Silva TG, González-Lozano KJ, Caldas IS,  
822 Gonçalves RV, et al. Thioridazine aggravates skeletal myositis, systemic and liver  
823 inflammation in Trypanosoma cruzi-infected and benznidazole-treated mice. *Int*  
824 *Immunopharmacol.* 2020;85: 106611. doi:10.1016/j.intimp.2020.106611



- 825 41. Molina HA, Cardoni RL, Rimoldi MT. The neuromuscular pathology of experimental  
826 Chagas' disease. *J Neurol Sci.* 1987;81: 287–300. doi:10.1016/0022-510x(87)90104-3
- 827 42. Monteón VM, Furuzawa-Carballeda J, Alexandre-Aguilar R, Aranda-Fraustro A, Rosales-  
828 Encina JL, Reyes PA. American trypanosomiasis: in situ and generalized features of  
829 parasitism and inflammation kinetics in a murine model. *Exp Parasitol.* 1996;83: 267–  
830 274. doi:10.1006/expr.1996.0074
- 831 43. Weaver JD, Hoffman VJ, Roffe E, Murphy PM. Low-Level Parasite Persistence Drives  
832 Vasculitis and Myositis in Skeletal Muscle of Mice Chronically Infected with *Trypanosoma*  
833 *cruzi*. *Infect Immun.* 2019;87: e00081-19. doi:10.1128/IAI.00081-19
- 834 44. Araujo Furlan CL, Tosello Boari J, Rodriguez C, Canale FP, Fiocca Vernengo F, Boccardo S,  
835 et al. Limited Foxp3+ Regulatory T Cells Response During Acute *Trypanosoma cruzi*  
836 Infection Is Required to Allow the Emergence of Robust Parasite-Specific CD8+ T Cell  
837 Immunity. *Front Immunol.* 2018;9: 2555. doi:10.3389/fimmu.2018.02555
- 838 45. Tosello Boari J, Amezcua Vesely MC, Bermejo DA, Ramello MC, Montes CL, Cejas H, et al.  
839 IL-17RA signaling reduces inflammation and mortality during *Trypanosoma cruzi* infection  
840 by recruiting suppressive IL-10-producing neutrophils. *PLoS Pathog.* 2012;8: e1002658.  
841 doi:10.1371/journal.ppat.1002658
- 842 46. Ramirez-Archila MV, Muñiz J, Virgen-Ortiz A, Newton-Sánchez O, Melnikov VG,  
843 Dobrovinskaya OR. *Trypanosoma cruzi*: correlation of muscle lesions with contractile  
844 properties in the acute phase of experimental infection in mice (*Mus musculus*). *Exp*  
845 *Parasitol.* 2011;128: 301–308. doi:10.1016/j.exppara.2011.02.012
- 846 47. Tosello Boari J, Araujo Furlan CL, Fiocca Vernengo F, Rodriguez C, Ramello MC, Amezcua  
847 Vesely MC, et al. IL-17RA-Signaling Modulates CD8+ T Cell Survival and Exhaustion During  
848 *Trypanosoma cruzi* Infection. *Front Immunol.* 2018;9: 2347.  
849 doi:10.3389/fimmu.2018.02347
- 850 48. Koh B, Ulrich BJ, Nelson AS, Panangipalli G, Kharwadkar R, Wu W, et al. Bcl6 and Blimp1  
851 reciprocally regulate ST2+ Treg-cell development in the context of allergic airway  
852 inflammation. *J Allergy Clin Immunol.* 2020;146: 1121-1136.e9.  
853 doi:10.1016/j.jaci.2020.03.002
- 854 49. Molofsky AB, Van Gool F, Liang H-E, Van Dyken SJ, Nussbaum JC, Lee J, et al. Interleukin-  
855 33 and Interferon- $\gamma$  Counter-Regulate Group 2 Innate Lymphoid Cell Activation during  
856 Immune Perturbation. *Immunity.* 2015;43: 161–174. doi:10.1016/j.immuni.2015.05.019
- 857 50. Siede J, Fröhlich A, Datsi A, Hegazy AN, Varga DV, Holeccka V, et al. IL-33 Receptor-  
858 Expressing Regulatory T Cells Are Highly Activated, Th2 Biased and Suppress CD4 T Cell  
859 Proliferation through IL-10 and TGF $\beta$  Release. *PLoS One.* 2016;11: e0161507.  
860 doi:10.1371/journal.pone.0161507
- 861 51. Vasanthakumar A, Chisanga D, Blume J, Gloury R, Britt K, Henstridge DC, et al. Sex-  
862 specific adipose tissue imprinting of regulatory T cells. *Nature.* 2020;579: 581–585.  
863 doi:10.1038/s41586-020-2040-3
- 864 52. Vasanthakumar A, Moro K, Xin A, Liao Y, Gloury R, Kawamoto S, et al. The transcriptional  
865 regulators IRF4, BATF and IL-33 orchestrate development and maintenance of adipose  
866 tissue-resident regulatory T cells. *Nat Immunol.* 2015;16: 276–285. doi:10.1038/ni.3085

- 867 53. Muñoz-Rojas AR, Mathis D. Tissue regulatory T cells: regulatory chameleons. *Nat Rev*  
868 *Immunol.* 2021;21: 597–611. doi:10.1038/s41577-021-00519-w
- 869 54. Abbas AK, Trotta E, R Simeonov D, Marson A, Bluestone JA. Revisiting IL-2: Biology and  
870 therapeutic prospects. *Sci Immunol.* 2018;3: eaat1482. doi:10.1126/sciimmunol.aat1482
- 871 55. Griesenauer B, Paczesny S. The ST2/IL-33 Axis in Immune Cells during Inflammatory  
872 Diseases. *Front Immunol.* 2017;8: 475. doi:10.3389/fimmu.2017.00475
- 873 56. de Oliveira MFA, Talvani A, Rocha-Vieira E. IL-33 in obesity: where do we go from here?  
874 *Inflamm Res.* 2019;68: 185–194. doi:10.1007/s00011-019-01214-2
- 875 57. Li C, Wang G, Sivasami P, Ramirez RN, Zhang Y, Benoist C, et al. Interferon- $\alpha$ -producing  
876 plasmacytoid dendritic cells drive the loss of adipose tissue regulatory T cells during  
877 obesity. *Cell Metab.* 2021;33: 1610-1623.e5. doi:10.1016/j.cmet.2021.06.007
- 878 58. Morrow KN, Coopersmith CM, Ford ML. IL-17, IL-27, and IL-33: A Novel Axis Linked to  
879 Immunological Dysfunction During Sepsis. *Front Immunol.* 2019;10: 1982.  
880 doi:10.3389/fimmu.2019.01982
- 881 59. Junqueira C, Caetano B, Bartholomeu DC, Melo MB, Ropert C, Rodrigues MM, et al. The  
882 endless race between *Trypanosoma cruzi* and host immunity: lessons for and beyond  
883 Chagas disease. *Expert Rev Mol Med.* 2010;12: e29. doi:10.1017/S1462399410001560
- 884 60. Paroli AF, Gonzalez PV, Díaz-Luján C, Onofrio LI, Arocena A, Cano RC, et al. NLRP3  
885 Inflammasome and Caspase-1/11 Pathway Orchestrate Different Outcomes in the Host  
886 Protection Against *Trypanosoma cruzi* Acute Infection. *Front Immunol.* 2018;9: 913.  
887 doi:10.3389/fimmu.2018.00913
- 888 61. Endo Y, Karvar M, Sinha I. Muscle Cryoinjury and Quantification of Regenerating  
889 Myofibers in Mice. *Bio Protoc.* 2021;11: e4036. doi:10.21769/BioProtoc.4036
- 890 62. Klose CSN, Artis D. Innate lymphoid cells as regulators of immunity, inflammation and  
891 tissue homeostasis. *Nat Immunol.* 2016;17: 765–774. doi:10.1038/ni.3489
- 892 63. Tait Wojno ED, Beamer CA. Isolation and Identification of Innate Lymphoid Cells (ILCs) for  
893 Immunotoxicity Testing. *Methods Mol Biol.* 2018;1803: 353–370. doi:10.1007/978-1-  
894 4939-8549-4\_21
- 895 64. Molofsky AB, Savage AK, Locksley RM. Interleukin-33 in Tissue Homeostasis, Injury, and  
896 Inflammation. *Immunity.* 2015;42: 1005–1019. doi:10.1016/j.immuni.2015.06.006
- 897 65. Verri WA, Guerrero ATG, Fukada SY, Valerio DA, Cunha TM, Xu D, et al. IL-33 mediates  
898 antigen-induced cutaneous and articular hypernociception in mice. *Proc Natl Acad Sci U S*  
899 *A.* 2008;105: 2723–2728. doi:10.1073/pnas.0712116105
- 900 66. Tarleton RL. CD8+ T cells in *Trypanosoma cruzi* infection. *Semin Immunopathol.* 2015;37:  
901 233–238. doi:10.1007/s00281-015-0481-9
- 902 67. Chen X, Li M, Chen B, Wang W, Zhang L, Ji Y, et al. Transcriptome sequencing and analysis  
903 reveals the molecular mechanism of skeletal muscle atrophy induced by denervation.  
904 *Ann Transl Med.* 2021;9: 697. doi:10.21037/atm-21-1230

- 905 68. Sastourné-Arrey Q, Mathieu M, Contreras X, Monferran S, Bourlier V, Gil-Ortega M, et al.  
906 Adipose tissue is a source of regenerative cells that augment the repair of skeletal muscle  
907 after injury. *Nat Commun.* 2023;14: 80. doi:10.1038/s41467-022-35524-7
- 908 69. Yan Z, Choi S, Liu X, Zhang M, Schageman JJ, Lee SY, et al. Highly coordinated gene  
909 regulation in mouse skeletal muscle regeneration. *J Biol Chem.* 2003;278: 8826–8836.  
910 doi:10.1074/jbc.M209879200
- 911 70. Cayrol C, Girard J-P. Interleukin-33 (IL-33): A critical review of its biology and the  
912 mechanisms involved in its release as a potent extracellular cytokine. *Cytokine.*  
913 2022;156: 155891. doi:10.1016/j.cyto.2022.155891
- 914 71. Liew FY, Girard J-P, Turnquist HR. Interleukin-33 in health and disease. *Nat Rev Immunol.*  
915 2016;16: 676–689. doi:10.1038/nri.2016.95
- 916 72. Lüthi AU, Cullen SP, McNeela EA, Duriez PJ, Afonina IS, Sheridan C, et al. Suppression of  
917 interleukin-33 bioactivity through proteolysis by apoptotic caspases. *Immunity.* 2009;31:  
918 84–98. doi:10.1016/j.immuni.2009.05.007
- 919 73. Cohen ES, Scott IC, Majithiya JB, Rapley L, Kemp BP, England E, et al. Oxidation of the  
920 alarmin IL-33 regulates ST2-dependent inflammation. *Nat Commun.* 2015;6: 8327.  
921 doi:10.1038/ncomms9327
- 922 74. Braband KL, Kaufmann T, Floess S, Zou M, Huehn J, Delacher M. Stepwise acquisition of  
923 unique epigenetic signatures during differentiation of tissue Treg cells. *Front Immunol.*  
924 2022;13: 1082055. doi:10.3389/fimmu.2022.1082055
- 925 75. Frisbee AL, Saleh MM, Young MK, Leslie JL, Simpson ME, Abhyankar MM, et al. IL-33  
926 drives group 2 innate lymphoid cell-mediated protection during *Clostridium difficile*  
927 infection. *Nat Commun.* 2019;10: 2712. doi:10.1038/s41467-019-10733-9
- 928 76. Ngo Thi Phuong N, Palmieri V, Adamczyk A, Klopffleisch R, Langhorst J, Hansen W, et al. IL-  
929 33 Drives Expansion of Type 2 Innate Lymphoid Cells and Regulatory T Cells and Protects  
930 Mice From Severe, Acute Colitis. *Front Immunol.* 2021;12: 669787.  
931 doi:10.3389/fimmu.2021.669787
- 932 77. Uddin MJ, Leslie JL, Burgess SL, Oakland N, Thompson B, Abhyankar M, et al. The IL-33-  
933 ILC2 pathway protects from amebic colitis. *Mucosal Immunol.* 2022;15: 165–175.  
934 doi:10.1038/s41385-021-00442-2
- 935 78. Aparicio-Domingo P, Cannelle H, Buechler MB, Nguyen S, Kallert SM, Favre S, et al.  
936 Fibroblast-derived IL-33 is dispensable for lymph node homeostasis but critical for CD8 T-  
937 cell responses to acute and chronic viral infection. *Eur J Immunol.* 2021;51: 76–90.  
938 doi:10.1002/eji.201948413
- 939 79. Bonilla WV, Fröhlich A, Senn K, Kallert S, Fernandez M, Johnson S, et al. The alarmin  
940 interleukin-33 drives protective antiviral CD8<sup>+</sup> T cell responses. *Science.* 2012;335: 984–  
941 989. doi:10.1126/science.1215418
- 942 80. Marx A-F, Kallert SM, Brunner TM, Villegas JA, Geier F, Fixemer J, et al. The alarmin  
943 interleukin-33 promotes the expansion and preserves the stemness of Tcf-1<sup>+</sup> CD8<sup>+</sup> T cells  
944 in chronic viral infection. *Immunity.* 2023;56: 813–828.e10.  
945 doi:10.1016/j.immuni.2023.01.029

- 946 81. Belkaid Y, Tarbell K. Regulatory T cells in the control of host-microorganism interactions  
947 (\*). *Annu Rev Immunol.* 2009;27: 551–589.  
948 doi:10.1146/annurev.immunol.021908.132723
- 949 82. Rocha IH, Ferreira Marques AL, Moraes GV, Alves da Silva DA, Silva MV da, Rodrigues V,  
950 et al. Metabolic and immunological evaluation of patients with indeterminate and  
951 cardiac forms of Chagas disease. *Medicine (Baltimore).* 2020;99: e23773.  
952 doi:10.1097/MD.00000000000023773
- 953 83. Albareda MC, Olivera GC, Laucella SA, Alvarez MG, Fernandez ER, Lococo B, et al. Chronic  
954 human infection with *Trypanosoma cruzi* drives CD4+ T cells to immune senescence. *J*  
955 *Immunol.* 2009;183: 4103–4108. doi:10.4049/jimmunol.0900852
- 956 84. Poncini CV, Giménez G, Pontillo CA, Alba-Soto CD, de Isola ELD, Piazzón I, et al. Central  
957 role of extracellular signal-regulated kinase and Toll-like receptor 4 in IL-10 production in  
958 regulatory dendritic cells induced by *Trypanosoma cruzi*. *Mol Immunol.* 2010;47: 1981–  
959 1988. doi:10.1016/j.molimm.2010.04.016
- 960 85. Piron M, Fisa R, Casamitjana N, López-Chejade P, Puig L, Vergés M, et al. Development of  
961 a real-time PCR assay for *Trypanosoma cruzi* detection in blood samples. *Acta Trop.*  
962 2007;103: 195–200. doi:10.1016/j.actatropica.2007.05.019
- 963 86. Fiocca Vernengo F, Beccaria CG, Araujo Furlan CL, Tosello Boari J, Almada L, Gorosito  
964 Serrán M, et al. CD8+ T Cell Immunity Is Compromised by Anti-CD20 Treatment and  
965 Rescued by Interleukin-17A. *mBio.* 2020;11: e00447-20. doi:10.1128/mBio.00447-20
- 966 87. Souza DG, Cara DC, Cassali GD, Coutinho SF, Silveira MR, Andrade SP, et al. Effects of the  
967 PAF receptor antagonist UK74505 on local and remote reperfusion injuries following  
968 ischaemia of the superior mesenteric artery in the rat. *Br J Pharmacol.* 2000;131: 1800–  
969 1808. doi:10.1038/sj.bjp.0703756
- 970 88. Frankish A, Diekhans M, Ferreira A-M, Johnson R, Jungreis I, Loveland J, et al. GENCODE  
971 reference annotation for the human and mouse genomes. *Nucleic Acids Res.* 2019;47:  
972 D766–D773. doi:10.1093/nar/gky955
- 973 89. Patro R, Duggal G, Love MI, Irizarry RA, Kingsford C. Salmon provides fast and bias-aware  
974 quantification of transcript expression. *Nat Methods.* 2017;14: 417–419.  
975 doi:10.1038/nmeth.4197
- 976 90. Chen EY, Tan CM, Kou Y, Duan Q, Wang Z, Meirelles GV, et al. Enrichr: interactive and  
977 collaborative HTML5 gene list enrichment analysis tool. *BMC Bioinformatics.* 2013;14:  
978 128. doi:10.1186/1471-2105-14-128
- 979 91. Kuleshov MV, Jones MR, Rouillard AD, Fernandez NF, Duan Q, Wang Z, et al. Enrichr: a  
980 comprehensive gene set enrichment analysis web server 2016 update. *Nucleic Acids Res.*  
981 2016;44: W90-97. doi:10.1093/nar/gkw377
- 982 92. Xie Z, Bailey A, Kuleshov MV, Clarke DJB, Evangelista JE, Jenkins SL, et al. Gene Set  
983 Knowledge Discovery with Enrichr. *Current Protocols.* 2021;1: e90. doi:10.1002/cpz1.90
- 984 93. Deacon RMJ. Measuring the strength of mice. *J Vis Exp.* 2013; 2610. doi:10.3791/2610
- 985

986 **FIGURE CAPTIONS**

987 **Fig 1: Characterization of muscular and systemic tissue damage during acute *T. cruzi* infection.**

988 Foxp3-GFP mice were infected with *T. cruzi* and tissue damage and infection progression were  
989 evaluated at different days post infection (dpi). (A) Kinetics of parasite counts in blood. (B)  
990 Kinetics of *T. cruzi* satellite DNA quantification in skeletal muscle (SM), heart, liver and spleen.  
991 (C) Kinetics of total spleen CD45+ cell count. (D) Representative Hematoxylin-Eosin stain of  
992 quadriceps muscle from non-infected (NI) and infected (INF) (21 dpi) mice (N = 4-7). Black arrow:  
993 parasites nest, blue arrows: necrotic muscle fibers, orange arrows: calcified muscle fibers.  
994 Magnification = 10X. INF images represent different areas from the same sample. (E) Kinetics of  
995 total SM CD45+ cell count. (F-G) Whole quadriceps SM RNAseq data analysis from NI and INF  
996 animals; N = 3 per group. (F) Non-supervised pathway analysis of the differentially expressed  
997 genes between INF and NI SM. Bars show the top-ten pathways upregulated in INF SM with red  
998 arrows highlighting pathways related to SM physiology. (G) Volcano plots display differentially  
999 expressed genes between INF and NI SM. According to (F), genes associated with oxidative  
1000 phosphorylation (left), myogenesis (center) and adipogenesis (right) pathways are highlighted  
1001 in red. (H) Kinetics of plasma CPK, CPK-MB, LDH, GOT and GPT activities, and glucose  
1002 concentration. (A, C, E and H) Data is presented as mean  $\pm$  SEM; N = 4-15 per dpi. Statistical  
1003 significance was determined by one-way ANOVA. P values are relative to 0 dpi: \*p < 0.05; \*\*p <  
1004 0.01; \*\*\*p < 0.001; \*\*\*\*p < 0.0001. (B) Data are presented as mean and values are normalized  
1005 to spleen tissue parasitism at 10 dpi; N = 4-5 per dpi. (A-E and H) Data were collected from 2-3  
1006 independent experiments.

1007

1008 **Fig 2: Tissue repair Tregs are reduced in target tissues and lymphoid organs during acute *T.***

1009 ***cruzi* infection.** Tissue repair Tregs (trTregs) were studied by flow cytometry in tissues from *T.*  
1010 *cruzi* infected Foxp3-GFP mice at different days post infection (dpi). (A) Representative dot plots

1011 showing ST2 and KLRG-1 staining in total Tregs present in skeletal muscle (SM), liver and spleen  
1012 obtained from non-infected (NI) and infected (INF) (21 dpi) mice. ST2+ KLRG-1+ cells (pink gate)  
1013 were defined as trTregs. (B) Graphs displaying trTregs frequency within total Tregs (upper row)  
1014 and absolute number (bottom row) in different tissues from NI and INF animals. Bars indicate  
1015 the mean  $\pm$  SEM. For SM, squares represent pools with N=3 mice. For spleen and liver, circles  
1016 represent individual mice. (C) Heatmap displaying the relative expression or frequency of the  
1017 indicated markers in splenic trTregs (pink gate) or ST2- KLRG-1- Tregs (golden gate) as defined  
1018 in (A), evaluated in NI and INF animals (N=5-6). (D) Principal component analysis of data  
1019 presented in (C). (E) Kinetics of trTregs frequency within total Tregs (upper row) and absolute  
1020 number (bottom row) in SM, liver and spleen. Data are presented as mean  $\pm$  SEM; N = 6-21 per  
1021 dpi. (B, E) For SM, cell counts are normalized to tissue weight. Statistical significance was  
1022 determined by Unpaired t test (B) and Kruskal-Wallis test (E). P values in (B) represent pairwise  
1023 comparisons, while in (E) are relative to 0 dpi: \*p < 0.05; \*\*p < 0.01; \*\*\*p < 0.001; \*\*\*\*p <  
1024 0.0001. (A-E) Data were collected from 2-3 independent experiments.

1025

1026 **Fig 3: IL-33 supplementation fails to prevent trTregs reduction in established infection.** (A) IL-  
1027 33 concentration in plasma and SM lysates obtained from Foxp3-GFP mice at different days post  
1028 infection (dpi). Muscle values were normalized to total protein content. Data are presented as  
1029 mean  $\pm$  SEM; N = 3-15 per dpi. (B) Representative dot plots showing ST2+ KLRG-1+ Tregs (trTregs)  
1030 frequency within total Tregs isolated from the spleen of non-infected (NI) and infected (INF) (21  
1031 dpi) Foxp3-GFP mice. Left plots correspond to uncultured Tregs, while middle and right plots  
1032 correspond to Tregs activated with anti-CD3+anti-CD28+IL-2 with or without rIL-33 for 72 hours.  
1033 (C) Experimental scheme illustrating the treatment of Foxp3-GFP mice with an established  
1034 infection with IL-33 or IL-33+IL-2. (D) Flow cytometry analysis of Tregs present in the spleen of  
1035 non-infected (NI) Foxp3-GFP mice 72 h after receiving 3 doses of intraperitoneal IL-33 or PBS as

1036 described in (C). Dot plots show the frequency of trTregs within total Tregs. (E) Graphs displaying  
1037 trTregs frequency within total Tregs (upper row) and absolute number (bottom row) in skeletal  
1038 muscle (SM), liver and spleen from INF animals (21 dpi) receiving intraperitoneal PBS, IL-33 or  
1039 IL-2/IL-33 as described in C. Bars indicate the mean  $\pm$  SEM. For each tissue, gray dashed lines  
1040 indicate the average of trTregs count in untreated NI mice. Statistical significance was  
1041 determined by Kruskal-Wallis test (A) and Mann-Whitney test (E). P values in (A) are relative to  
1042 0 dpi: \* $p < 0.05$ ; \*\* $p < 0.01$ ; while in (E) represent pairwise comparison. Data are representative  
1043 of two (A-B) and one (D-E) independent experiments.

1044

1045 **Fig 4: Inflammatory and microbial-derived signals are unable to restrict IL-33 mediated**  
1046 **expansion of trTregs *in vitro*.** (A) Soluble ST2 (sST2) concentration in plasma, as well as in spleen,  
1047 skeletal muscle (SM) and liver lysates obtained from Foxp3-GFP mice at different days post  
1048 infection (dpi). In spleen and SM, values were normalized to total protein content and are  
1049 presented as mean  $\pm$  SEM. In the liver, results from a 1/10 dilution of liver lysates are depicted  
1050 as absorbance units due to falling outside the assay's dynamic range, as indicated by the black  
1051 dashed line. Statistical significance was determined by one-way ANOVA in spleen and SM.  
1052 Representative of one experiment with N = 4-7 per dpi. ND: non-detectable. (B-C)  
1053 Representative dot plots showing ST2+ KLRG-1+ Tregs (trTregs) frequency within total Tregs  
1054 isolated from the spleen of non-infected (NI) Foxp3-GFP mice for 72 h with anti-CD3+anti-CD28  
1055 together with the addition of different cytokines as follow: IL-2; IL-2+IL-33 and IL2+IL33 plus:  
1056 cytokines associated to Th1 signals, innate signals, as well as conditioned media or transwell co-  
1057 cultures providing soluble spleen-derived signals (B) or microbial ligands (C), as indicated above  
1058 each plot. (B-C) Data were collected from 4 independent experiments. Spl: splenocytes, Tps:  
1059 trypomastigotes.

1060

1061 **Fig 5: Early rIL-33 administration expands trTregs and improve disease outcome in infected**  
1062 **mice.** Immune response and disease progression was evaluated in infected Foxp3-GFP mice  
1063 after receiving intraperitoneal IL-33 the day of infection and on 3 and 6 days post infection (dpi).  
1064 (A) Experimental scheme. (B) Representative dot plots showing ST2+ KLRG-1+ Tregs (trTregs)  
1065 frequency within total Tregs isolated from the skeletal muscle (SM) of PBS or IL-33-treated  
1066 infected mice. (C) Graphs displaying trTregs frequency within total Tregs in SM, liver and spleen  
1067 at 21 dpi. For SM, squares represent pools with N = 4-5. For spleen and liver, circles represent  
1068 individual mice. (D) Heatmap showing relative values corresponding to parameters of disease  
1069 progression at 21 dpi. Each column represents one mouse. (E) Representative dot plots  
1070 illustrating type 2 innate lymphoid cells (ILC2) frequency within CD45+ CD4- CD8- Lin (CD3, CD19,  
1071 NK1.1, CD11c)- CD11b- cells. Graphs correspond to SM from PBS or IL-33-treated infected  
1072 mouse. (F) ILC2 frequencies within Live CD45+ cells in SM, liver and spleen at 21dpi. (G)  
1073 Representative dot plots showing TSKB20/K<sup>b</sup> staining in SM CD8+ cells from PBS or IL-33-treated  
1074 infected mice. (H) Percentage of parasite-specific CD8+ T cells in SM, liver and spleen at 21dpi.  
1075 (I) *T. cruzi* satellite DNA quantification in SM, heart and liver at 21 dpi. (C, F, H and I) Bars  
1076 represent the mean  $\pm$  SEM. Statistical significance was determined as follow: Mann-Whitney  
1077 test for SM and unpaired t test for liver and spleen (A); unpaired t test (F and H) and Mann-  
1078 Whitney test (I). Data are representative of two (C, D, H and I) and one (F) independent  
1079 experiments.

1080

## 1081 SUPPORTING INFORMATION

1082 **S1 Fig: Peripheral target tissues display inflammatory responses during acute *T. cruzi* infection.**  
1083 Inflammatory response was evaluated in *T. cruzi* infected Foxp3-GFP mice at different days post  
1084 infection (dpi). (A) Whole quadriceps muscle (SM) RNAseq data analysis from NI and INF mice as  
1085 described in Fig 1F-G; N = 3 per group. Volcano plots displaying differentially expressed genes



1086 (dots) between INF SM and NI SM. According to Figure 1F, genes associated with interferon  
1087 gamma response, interferon alpha response and complement pathways are highlighted in red.  
1088 (B) Number of CD45+ cells in heart and liver, determined by flow cytometry at different dpi. Data  
1089 are presented as mean  $\pm$  SEM; N = 4-9 per group. For liver, counts correspond to total leukocyte  
1090 numbers, whereas for heart, cell numbers are normalized to tissue weight. Statistical  
1091 significance was determined by one-way ANOVA and P values relative to 0 dpi. \* $p < 0.05$ ; \*\*\*\* $p$   
1092  $< 0.0001$ .

1093

1094 **S2 Fig: Tregs frequency is reduced in lymphoid and non-lymphoid target tissues during acute**  
1095 ***T. cruzi* infection.** Tregs response was evaluated by flow cytometry in spleen, liver, skeletal  
1096 muscle (SM) and heart from non-infected (NI) and infected (INF) (21 days post infection) Foxp3-  
1097 GFP mice. (A) Representative dot plots showing the frequency of Tregs (CD4+ Foxp3-GFP+)  
1098 within total CD4+ cells from each tissue. (B) Bars displaying Tregs frequency within total CD4+  
1099 cells as the mean  $\pm$  SEM. Circles represent individual mice; squares represent pools with 3-5  
1100 mice. For SM and heart, cell counts are normalized to tissue weight. Statistical significance was  
1101 determined by unpaired t test for spleen, liver and SM; and by Mann-Whitney test for heart. P  
1102 values are indicated in the graphs. (A-B) Data were collected from 3 independent experiments.

1103

1104 **S3 Fig: ST2+ KLRG-1+ Tregs from *T. cruzi* infected mice exhibit a phenotype compatible with**  
1105 ***bona fide* trTregs.** Flow cytometry phenotypic analysis of Tregs subsets present in the spleen of  
1106 non-infected (NI) or infected (INF) (21 dpi) Foxp3-GFP mice. Histograms show the expression of  
1107 each cell marker in ST2+ KLRG-1+ (pink) and ST2- KLRG-1- (golden) Tregs as defined in Fig 2A.  
1108 Numbers on top right corner of each plot indicate either mean fluorescence intensity or  
1109 frequency of positive cells for each marker.

1110

1111 **S4 Fig: IL-33 supplementation fails to prevent trTregs reduction in established *T. cruzi***  
1112 **infection.** (A) IL-33 concentration was evaluated in spleen and liver lysates obtained from Foxp3-  
1113 GFP mice at different days post infection (dpi). Values were normalized to total protein content.  
1114 Data are presented as mean  $\pm$  SEM; N = 4-12 per dpi. (B) GFPneg CD4+ conventional T cells  
1115 (Tconv) isolated from the spleen of non-infected (NI) and infected (INF) (21 dpi) Foxp3-GFP mice  
1116 were evaluated by flow cytometry. Representative dot plots showing ST2+ KLRG-1+ cells  
1117 frequency within total Tconv. Left plots correspond to uncultured Tconv, while middle and right  
1118 plots correspond to Tconv activated with anti-CD3+anti-CD23+IL-2 with or without rIL-33 for 72  
1119 hours. (C-E) Analysis of disease progression in INF mice treated with intraperitoneal IL-33 or IL-  
1120 33+IL-2 as described in Fig 3C. (C) Plasma LDH, GOT, GPT, CPK and CPK-MB activities, and glucose  
1121 concentration at 21 dpi. (D) Percentage of total body weight reduction at 21 dpi compared to 15  
1122 dpi. (E) Survival curve in the different experimental groups. (F, G) Representative plots depicting  
1123 the frequencies of GFP+ CD4+ Tregs cells (F, G) and ST2+ KLRG-1+ cells (G) in NI (F) and INF (G)  
1124 mice receiving intramuscular IL-33. Statistical significance was determined by Kruskal-Wallis test  
1125 (A), Mann-Whitney test (C-D), Mantel-Cox test (E) and Wilcoxon test (G). P values in (A) are  
1126 relative to 0 dpi: \*\*\*\*p < 0.0001; while in (C-D and G) represent pairwise comparisons; ns: non-  
1127 significant.

1128

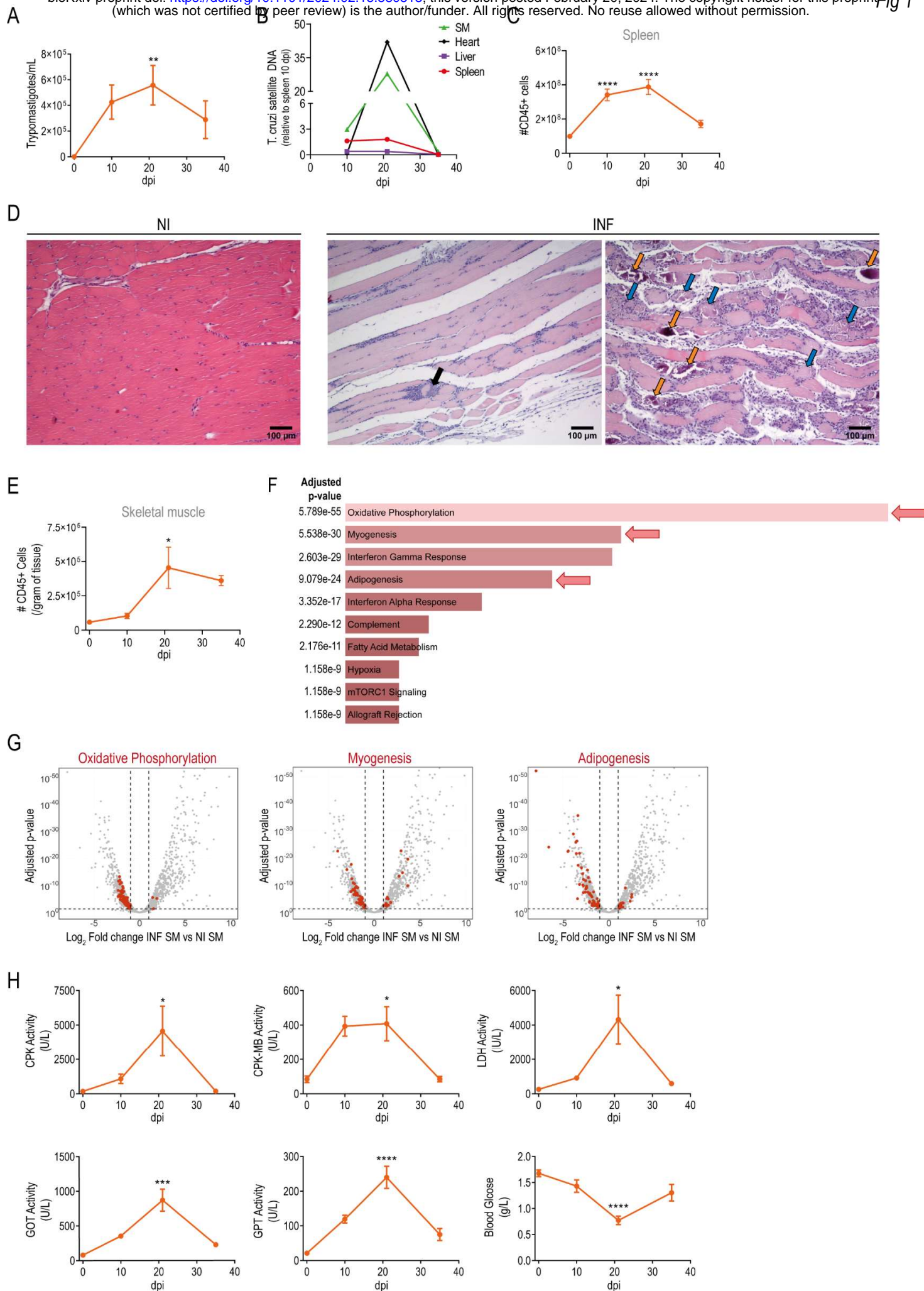
1129 **S5 Fig: Early rIL-33 administration improves the global health status without reducing SM**  
1130 **alterations during acute infection.** Immune response and disease progression was evaluated in  
1131 infected Foxp3-GFP mice after receiving intraperitoneal IL-33 the day of infection and on 3 and  
1132 6 days post infection (dpi). (A) trTregs count in skeletal muscle (SM), liver and spleen at 21 dpi.  
1133 For SM, squares represent pools with N=4-5. For spleen and liver, circles represent individual  
1134 mice. For each tissue, gray dashed lines indicate the average of trTregs count in untreated non-  
1135 infected (NI) mice. (B) Plasma LDH, GOT, CPK, GPT and CPK-MB activities, and glucose

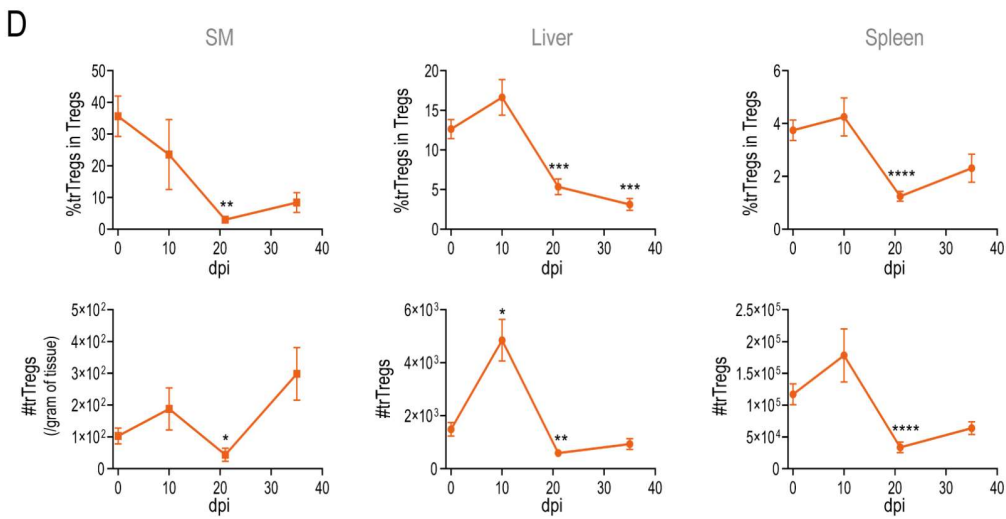
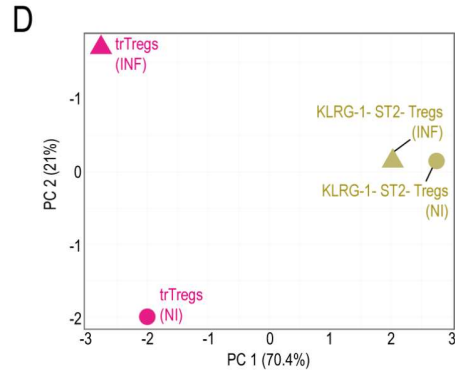
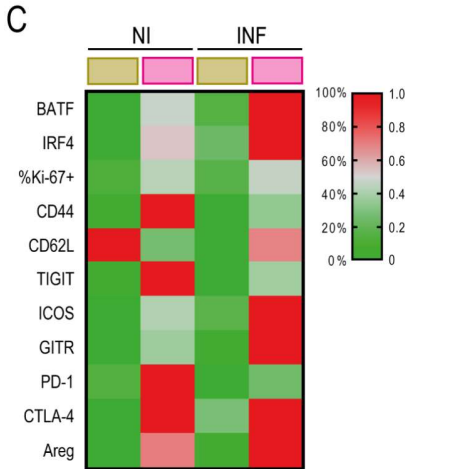
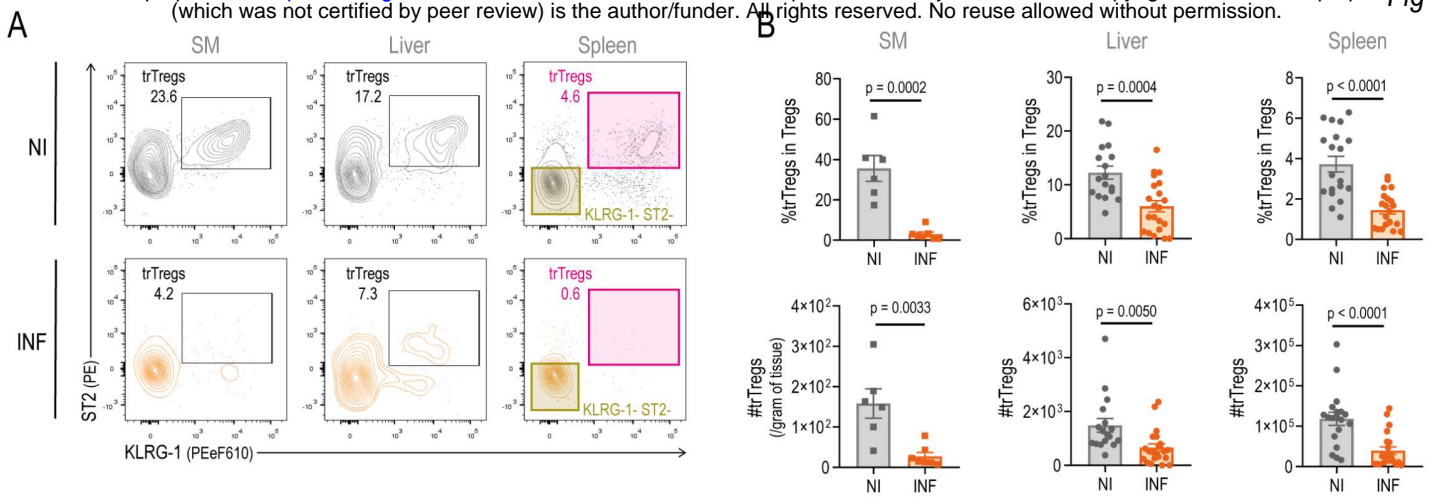
1136 concentration at 21 dpi. (C) Total body weight loss between 15 and 21 dpi. (D) Inverted screen  
1137 test (max: 120 seconds) and (E) Hematoxylin-Eosin stain of quadriceps muscle at 21 dpi. Images  
1138 are representative of N = 4. Black arrow: centrally nucleated muscular fibers. Magnification = 4X  
1139 (left) and 10X (right). (F) Gating strategy used to identify type 2 innate lymphoid cells (ILC2) as  
1140 CD45+ CD4- CD8- Lin (CD3, CD19, NK1.1, CD11c)- CD11b- CD127+ ST2+ cells. Dot plots are  
1141 representative of SM from IL-33-treated infected mouse. (G) ILC2 and (H) parasite-specific CD8+  
1142 cell count in SM, liver and spleen at 21 dpi. For SM, counts are normalized to tissue weight. (A-  
1143 D, G and H) Bars represent the mean  $\pm$  SEM. Statistical significance was determined as follow:  
1144 Mann-Whitney test for SM and unpaired t test for liver and spleen (A); unpaired t test (B-D, G  
1145 and H). (A-D, G and H) P values from pairwise comparison are indicated in the graphs. Data are  
1146 representative of two (A-D and H) and one (E and G) independent experiments.

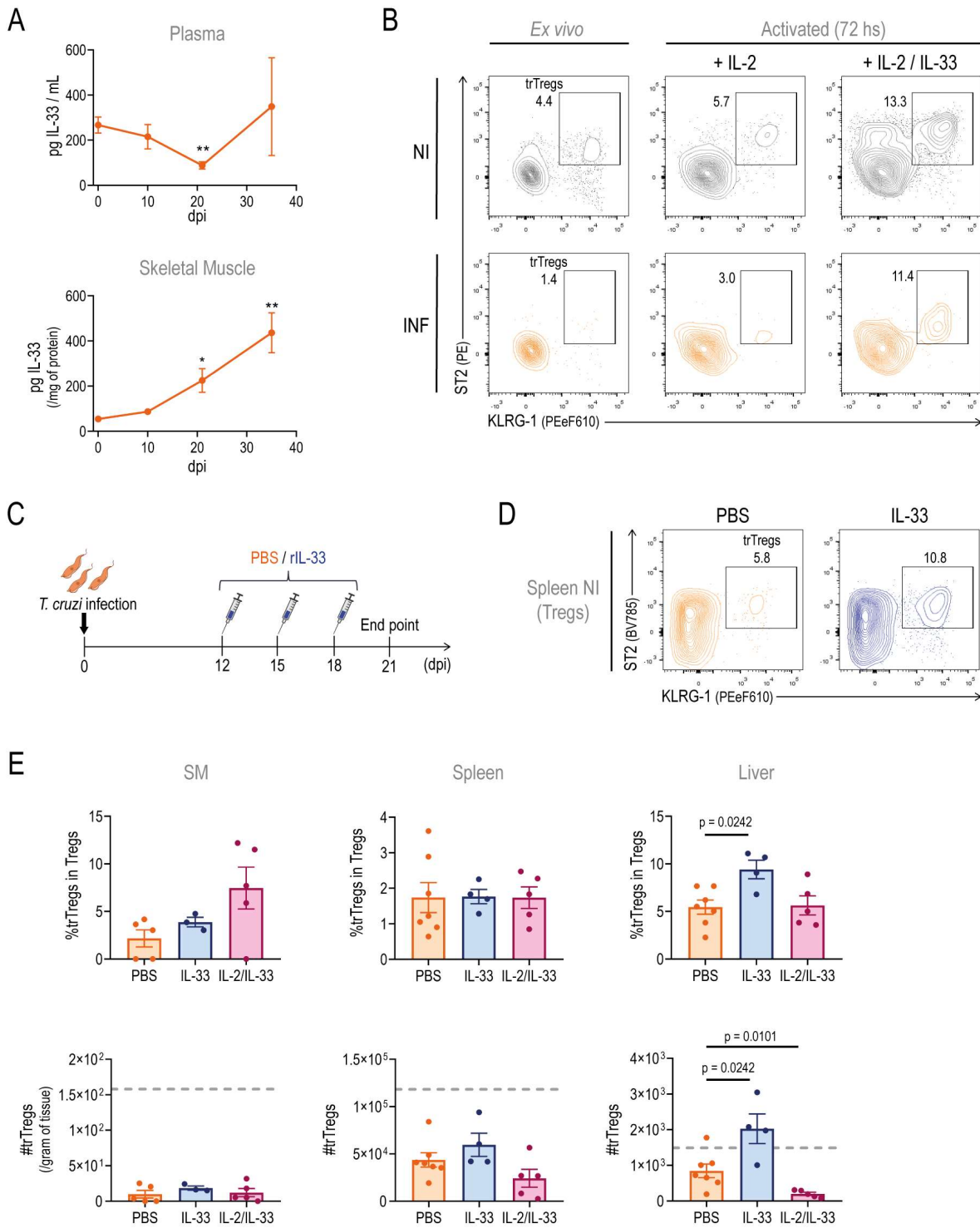
1147

1148 **S1 Table: List of genes associated with inflammatory response and skeletal muscle physiology.**

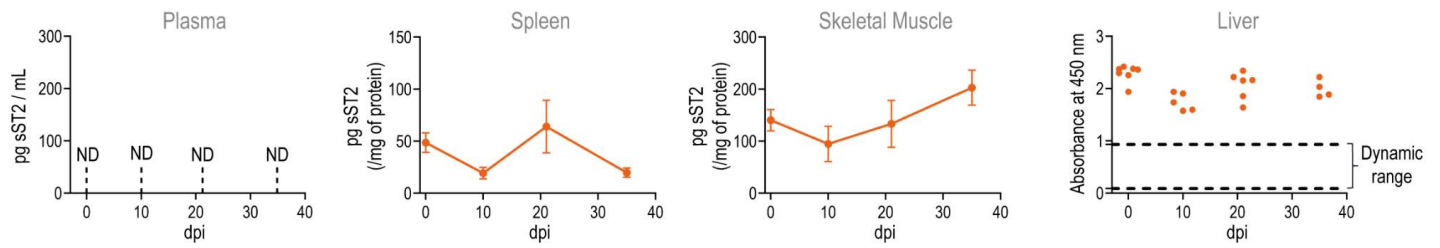
1149 Differentially expressed genes between infected (15 days post infection) and non-infected mice  
1150 are shown for each cellular pathway.



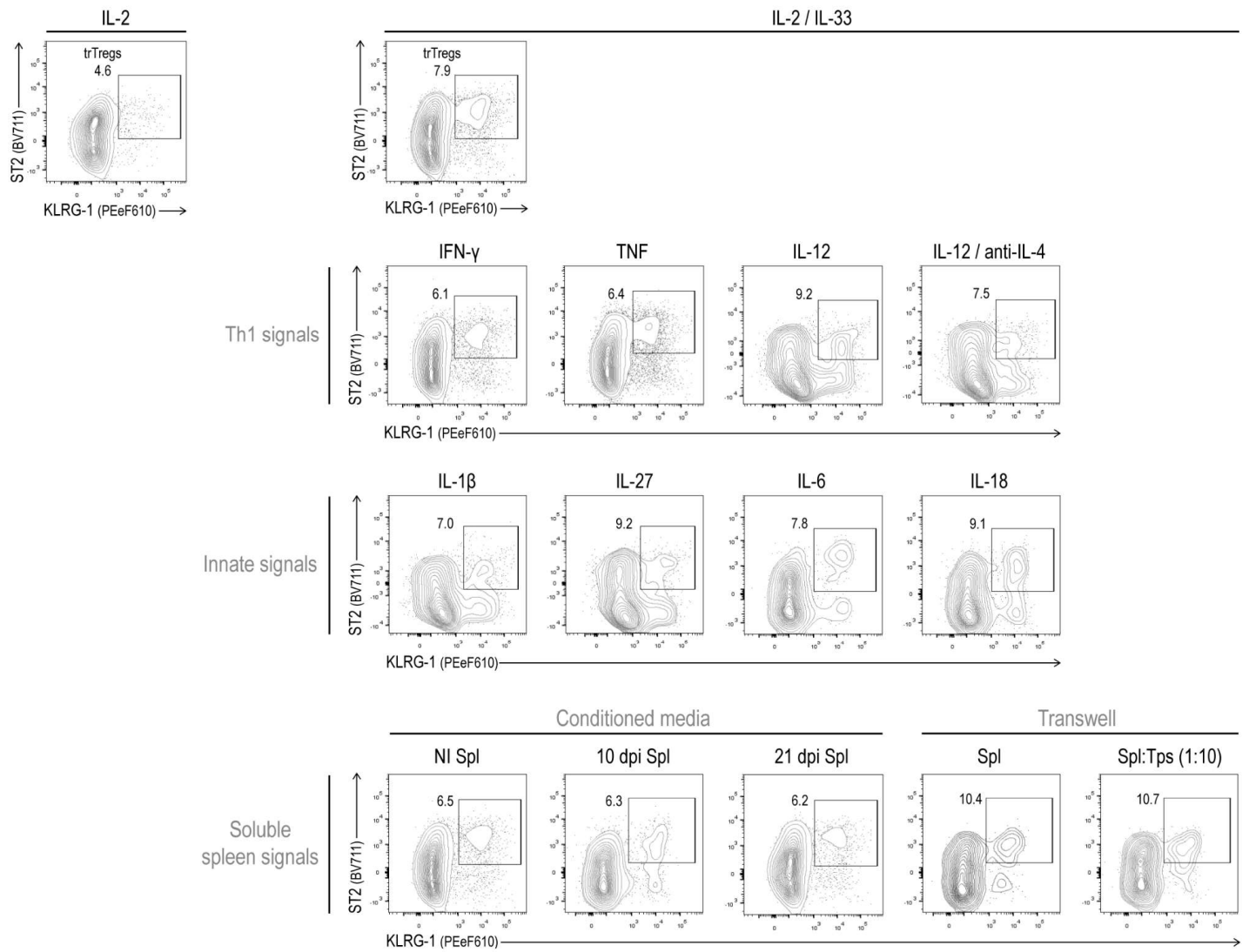




A



B



C

